

Mechanism of K^+ coupling in excitatory amino acid transporters

Inaugural-Dissertation

zur Erlangung des Doktorgrades
der Mathematisch-Naturwissenschaftlichen Fakultät
der Heinrich-Heine-Universität Düsseldorf

vorgelegt von

Daniel Kortzak
aus Mönchengladbach

Jülich, Februar 2017

aus dem Institute of Complex Systems – Zelluläre Biophysik
des Forschungszentrums Jülich

Gedruckt mit der Genehmigung der
Mathematisch-Naturwissenschaftlichen Fakultät der
Heinrich-Heine-Universität Düsseldorf

Referent: Prof. Dr. Christoph Fahlke
Korreferent: Prof. Dr. Holger Gohlke
Tag der mündlichen Prüfung: 14.12.2017

Für mapa

Contents

List of figures	III
List of tables	IV
1 Abstract	1
2 Zusammenfassung	2
3 Introduction	3
3.1 Excitatory amino acid transporters	3
3.2 EAAT structure and transport mechanism	5
3.3 K ⁺ interaction with EAATs	7
4 Material and Methods	10
4.1 MD simulations	10
4.1.1 Free energy calculations	11
4.1.2 Gating charge calculations	13
4.2 Experimental	14
4.2.1 Whole-cell patch-clamp	14
4.2.2 Microscale thermophoresis	15
4.3 Data analysis	15
5 Results	17
5.1 MD simulations of Glt _{Ph} reveal three binding sites	17
5.1.1 Spontaneous binding events in free MD	17
5.1.2 Extensive parallel MD simulations allow estimation of kinetic parameters	22
5.1.3 Free energy of K ⁺ binding by Umbrella sampling	29
5.1.4 Effect of K ⁺ binding on hairpin opening	35
5.1.5 HP opening determines K ⁺ coupling	38
5.1.6 Effects of <i>in silico</i> mutagenesis on free energy of binding	40
5.1.7 Voltage dependence of K ⁺ binding	44
5.2 Microscale thermophoresis of Glt _{Ph}	45
5.3 Experimental validation in EAAT2	47
5.3.1 Voltage jumps	47
5.3.2 Concentration jumps	51
6 Discussion	54
6.1 MD simulations reveal three potential binding sites	54
6.2 K ⁺ binding to K1 is coupled to hairpin closure	56
6.3 Glt _{Ph} interacts with K ⁺	57

6.4	Anion current recordings to examine K^+ interactions in EAAT2 .	58
6.5	Mutations in side-chains contributing to the K1 site affect one half-cycle, but leave the other intact	60
6.6	K^+ binding and K^+ bound translocation in EAAT2 are electrogenic	61
7	Conclusion	63
8	Bibliography	64
9	Publications	75
10	Abbreviations	76
11	Eidesstattliche Versicherung	78
12	Danksagung	79

List of Figures

3.1	EAAT transport cycle	4
3.2	Cartoon representation of the Glt _{Ph} structure	5
5.1	Representative spontaneous K ⁺ binding in MD	18
5.2	Overview of spontaneous binding events	20
5.3	Representative trajectories of binding events	21
5.4	Counting transitions between binding sites	23
5.5	State diagram for K1 binding	24
5.6	Principles of the umbrella sampling method	30
5.7	Free energy of K ⁺ binding	32
5.8	Hairpin dynamics	35
5.9	K ⁺ of HP opening	36
5.10	HP opening equilibrium in the apo states defines K ⁺ coupling in EAATs/Glt _{Ph}	39
5.11	Overview on spontaneous K ⁺ binding to D405N, N401A and D312N	41
5.12	Changes in free energy of K ⁺ binding by D405N, N401A and D312N	42
5.13	MST method	45
5.14	MST results	46
5.15	Anion current recordings of EAAT2, KNO ₃	48
5.16	Anion current recordings of EAAT2, NaNO ₃ +glu	49
5.17	K ⁺ dependence of EAAT2 anion currents	50
5.18	Current responses to fast K ⁺ application	52

List of Tables

5.1	Initial MD setups	17
5.2	Alignment of binding site forming residues	19
5.3	Number of transitions, inward-facing	25
5.4	Times spent in states, inward-facing	25
5.5	Transition rates, inward-facing	25
5.6	Equilibrium constants, inward-facing	26
5.7	Number of transitions, outward-facing	26
5.8	Times spent in states, outward-facing	26
5.9	Transition rates, outward-facing	27
5.10	Equilibrium constants, outward-facing	27
5.11	K_D from free MD	29
5.12	K_D from umbrella sampling	33
5.13	ΔG from umbrella sampling	33
5.14	Equilibrium constants of HP opening from free MD for different bound states	37
5.15	Equilibrium constants of HP opening from umbrella sampling simulations for different bound states	37
5.16	HP opening equilibrium in the apo states defines K^+ coupling in EAATs/Glt _{ph}	40
5.17	Free energy of K^+ binding to D405N, N401A and D312N	43
5.18	Gating charges	44

1. Abstract

Excitatory amino acid transporters (EAAT) terminate signal transmission in a glutamatergic synapse by removal of glutamate from the synaptic cleft. They harness the energy stored in pre-existing Na^+ and K^+ concentration gradients to drive secondary active glutamate transport. The K^+ -associated steps are rate-limiting for glutamate transport and represent promising pharmacological targets to modify EAAT transport rates in various human disease conditions.

We here combined extensive molecular dynamics (MD) simulations of prokaryotic EAAT homologs and patch-clamp recordings of mammalian EAAT2 to identify the molecular mechanisms of K^+ -coupled glutamate transport. Simulations of the prokaryotic homolog Glt_{Ph} show spontaneous association of K^+ to three distinct K^+ binding sites (K1–K3). K1 and K2 partly overlap with established Na^+ binding sites Na1 and Na2. Unbiased simulations suggest that association to K2 or K3 is a precondition for binding at K1, and that K^+ binding at K1 weakens binding at the other sites, while a K^+ ion remains stably bound at K1. Free energy calculations confirmed that K1 has the highest affinity. These results suggest that K1 serves as the final binding site that is occupied during the isomerization between inward- and outward-facing conformations.

We tested the predicted K^+ binding sites by combining *in silico* mutagenesis with *in vitro* mutagenesis, protein purification and microscale thermophoresis on Glt_{Ph} or heterologous expression and whole-cell patch-clamp recordings of EAAT2. Mutations that cause reduced free energies of binding in simulations also abolished K^+ binding of Glt_{Ph} and K^+ activated currents in EAAT2. We conclude that the K1 site is conserved in Glt_{Ph} and EAATs and that we can use simulations of Glt_{Ph} to investigate K^+ coupling in EAATs.

Simulations reveal that occupation of K1 closes the gate to the neurotransmitter binding site, which is a prerequisite for translocation across the membrane. Differences in the equilibrium between gate opening and closing account for obligate K^+ coupling in EAATs and K^+ independent transport in Glt_{Ph} . In conclusion, the combination of experimental and computational methods successfully resolved the K^+ binding sites as well as the mechanism of K^+ coupling in EAATs.

2. Zusammenfassung

Excitatory amino acid transporters (EAAT) beenden die Signalübertragung in glutamatergen Synapsen durch das Entfernen von Glutamat aus dem synaptischen Spalt. Sie nutzen die Energie, die in Na^+ - und K^+ -Konzentrationsgradienten gespeichert ist, für sekundär-aktiven Glutamattransport. Die mit K^+ assoziierten Schritte sind ratenlimitierend und stellen daher ein vielversprechendes pharmakologisches Ziel dar, um EAAT-Transportraten zu modifizieren.

In dieser Arbeit werden Molekulardynamiksimulationen (MD) von prokaryotischen EAAT-Homologen mit Patch-Clamp-Messungen von EAAT2 kombiniert, um die molekularen Mechanismen des K^+ -gekoppelten Glutamattransports zu identifizieren. Simulationen des prokaryotischen Homolog Glt_{Ph} zeigen spontane K^+ Assoziation an drei verschiedenen Bindestellen (K1–K3). K1 und K2 überlappen teilweise mit bekannten Na^+ Bindestellen. Weiter zeigen die Simulationen, dass Bindung an K2 oder K3 Voraussetzung für die Besetzung von K1 ist. Bindung an K1 schwächt die Bindung an den anderen Stellen, während die Bindung an K1 sehr stabil ist. Bindungsenergieberechnungen bestätigen, dass K1 die höchste Affinität hat. Diese Resultate suggerieren, dass K1 als finale Bindestelle dient, die während der Konformationsänderung von einwärts- nach auswärts-zeigendem Zustand besetzt ist.

Die vorhergesagten K^+ Bindestellen wurden durch die Kombination von *in silico* mit *in vitro* Mutagenese, Proteinaufreinigung und Microscale Thermophorese von Glt_{Ph} oder heterologer Expression und Patch-Clamp-Experimente von EAAT2 getestet. Mutationen die in MD Simulationen zu verringerten Bindungsenergien führen, zeigen auch im Experiment keine K^+ Bindung von Glt_{Ph} und keine K^+ aktivierten Ströme von EAAT2. Dies zeigt, dass die K1 Bindestelle in Glt_{Ph} und den EAATs konserviert ist, und dass Simulationen von Glt_{Ph} genutzt werden können, um die K^+ Kopplung in EAATs zu untersuchen.

Simulationen zeigen, dass die Bindung an K1 das Tor zu der Glutamat-Bindestelle schließt, was eine Bedingung für die Translokation über die Membran ist. Unterschiede im Gleichgewicht der Toröffnung und -schließung erklären strikte K^+ Kopplung der EAATs und K^+ unabhängigen Transport von Glt_{Ph} . Durch die Kombination von Experimenten und Simulationen wurden die K^+ -Bindestellen und der Mechanismus der K^+ Kopplung in EAATs identifiziert.

3. Introduction

3.1 Excitatory amino acid transporters

Glutamate is the major excitatory neurotransmitter in the mammalian central nervous system. To achieve a high signaling frequency as well as a low resting extracellular glutamate concentration, glutamate has not only to be released fast and to rapidly activate receptor proteins, but also to be rapidly removed from the synaptic cleft [1]. Prolonged time spans of high extracellular glutamate concentration are neurotoxic [2]. Several neurological diseases are associated with increased extracellular glutamate concentrations, among them are schizophrenia [3], Alzheimer's disease [4] and multiple sclerosis [5].

The proteins that perform this task are called excitatory amino acid transporters (EAATs), which belong to the solute carrier family 1 (SLC1). EAATs are secondary active transporters, i.e. they harness the energy stored in ionic concentration gradients across the cell membrane. In particular the transport of each glutamate molecule is coupled to co-transport of three sodium ions and one proton as well as the counter-transport of one potassium ion [6, 7, 8]. This stoichiometry leads to an inward movement of two positive charges per transported glutamate. EAATs are not only transporters, but also function as anion channels [9]. Anion permeation is not thermodynamically coupled to the transport of glutamate. However, gating of the channel is closely linked to transitions in the transport cycle and channel opening occurs from intermediate transporter conformations [10, 11]. The physiological role of this second function of EAATs was long unknown. It was proposed to be involved in shaping the excitability of a neuron [12] or a mechanism that compensates for the positive charge that moves into the cell with each transported glutamate. Recently, a major role of EAAT1 and EAAT2 anion channels in setting the internal chloride concentration in Bergmann glia cells was discovered [13].

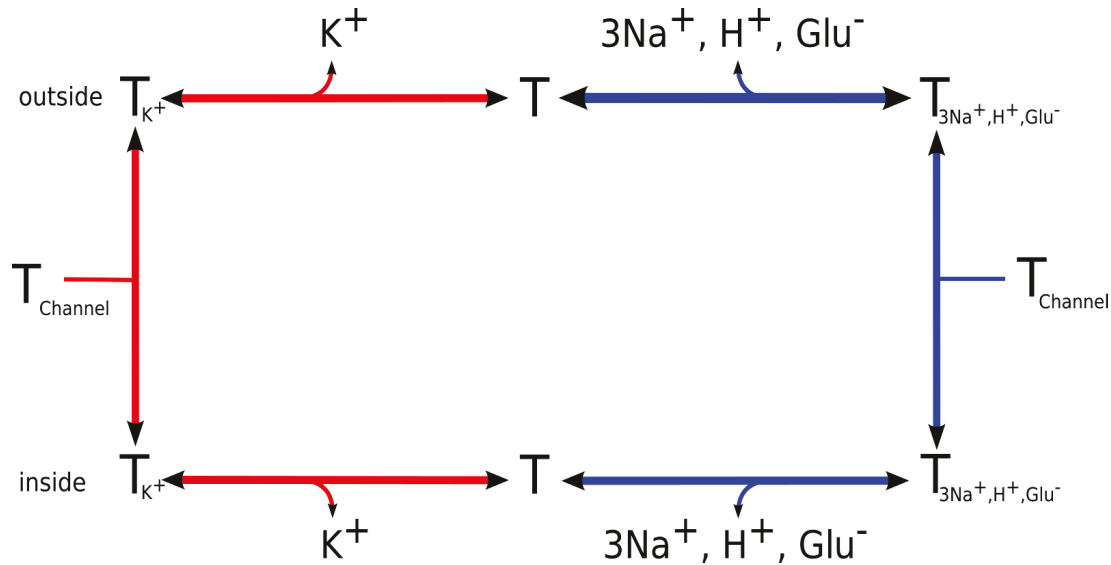


Figure 3.1: EAAT transport cycle. *Simplified state diagram of the EAAT transport cycle. Under physiological conditions transporters run in clockwise direction. The full cycle can be partitioned into two half-cycles. Glutamate bound transitions are colored in blue, potassium bound transitions are colored in red. This strict separation allows to measure each half-cycle in isolation by the use of appropriate ionic conditions.*

There are five known mammalian EAAT isoforms (EAAT1–5) [14] that differ in transport rate and channel activity [15] as well as in expression pattern. EAAT1 is only expressed in glia cells, while EAAT2 is expressed in glia cells and in neurons [14]. EAAT3 and EAAT4 are expressed in neurons where they can be found in dendrites and spines [16]. EAAT5 is a retinal glutamate transporter and is expressed in photoreceptors and bipolar cells [17].

The most important isoforms for glutamate uptake in glia and neurons are EAAT1–3, whereas EAAT4 and EAAT5 have a slow cycling time [15] and are better described as glutamate-gated anion channel. More than 90% of glutamate uptake into glia cells is mediated by EAAT2 [18], which thus represents the most important isoform. The importance of EAAT2 is corroborated by EAAT2 knock-out mouse models with most severe phenotype, i.e. spontaneous lethal seizures [19], as compared to the other isoforms [20, 21, 22]. There are also known mutations that modify EAAT function and are associated with neurological diseases such as ataxia or Tourette syndrome [23, 24, 25].

3.2 EAAT structure and transport mechanism

Glt_{Ph} is a EAAT homolog from the archaeon *Pyrococcus horikoshii* that has successfully served as a structural model for EAATs for more than ten years now. Glt_{Ph} is assembled as a trimeric protein that is build from three identical subunits [26] (Figure 3.2).

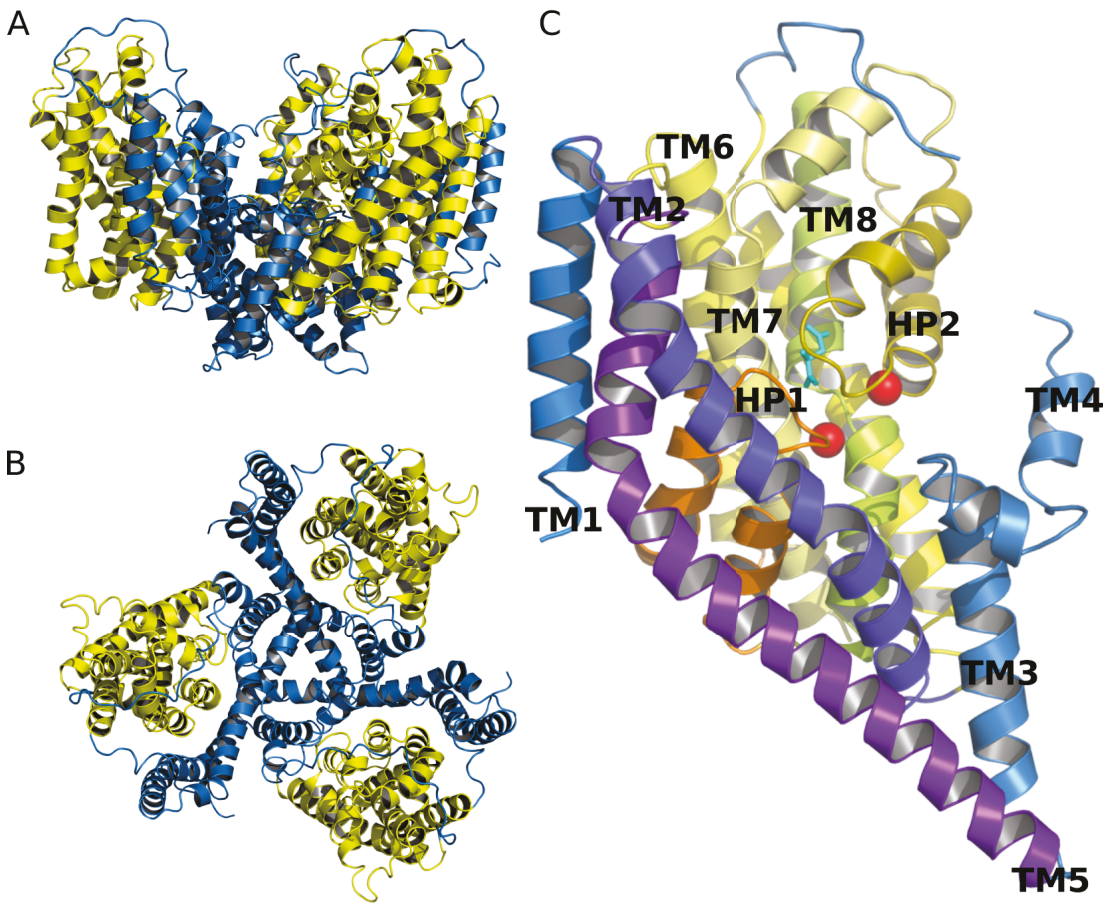


Figure 3.2: Cartoon representation of the Glt_{Ph} structure. **A**, View from the membrane plane on the trimer. **B**, Top view on the trimer. The trimerization domain is colored blue and the transport domain yellow. **C**, Topology of a single monomer with two sodium ions and aspartate bound (PDB ID 2NWX). The bound sodium ions are represented as red spheres and aspartate is represented as cyan sticks. The trimerization domain consists of TM1, TM2, TM4, and TM5. The transport domain consists of TM3, TM6, TM7, TM8, HP1, and HP2.

Each subunit performs the complete uptake cycle independent on the other monomers [27, 28, 29]. The monomer consists of eight transmembrane (TM) helices and two hairpin (HP) loops (Figure 3.2). Transport is based on the movement of one domain, whereas the rest of the subunit anchors the protein in the membrane and mediates the inter subunits interactions [30] (Figure 3.2). The transport domain binds the substrates and performs an elevator-like movement to alternatively expose the binding site to the intra- resp. extracellular compartment. The two hairpins that are part of the transport domain form the gate to the substrate binding sites that are buried under HP2. Opening of the gate, which is coupled to the movement of HP2, is necessary for substrate binding. This gate is also the main determinant for the transition of the transport domain: transitions between inward- and outward-facing states are only possible with a closed HP2 gate [31].

The published structures spawned a series of simulational studies addressing the mechanisms of substrate binding and translocation as well as the molecular basis of anion conduction. All this work supports the notion that Glt_{Ph} represents an excellent model for the glutamate and sodium sites in EAATs as well as the EAAT anion channel.

The first crystal structures showed only two of the three sodium sites and used thallium as a reporter for sodium binding sites [32]. Following this, a series of simulational studies addressed the issue of the third sodium site [33, 34, 35]. Several candidate sites were proposed and tested via free energy of binding simulations. Very recently a new structure was published which for the first time showed all three sodium sites occupied [36]. This structure confirmed the results of the prior MD studies [35]. The results found in computer simulations account for experimental data in EAATs demonstrating that computer simulations of Glt_{Ph} are a viable tool to get insight into biological processes in EAATs at atomistic resolution.

Experimental observations indicated that two sodiums bind before glutamate and one after. Molecular dynamics (MD) simulations allowed to get an atomistic view of the underlying processes. Binding of the first two sodiums induced movement of HP2, opening the gate to the substrate binding site. After binding of glutamate another sodium binds and closes the gate [34].

Aspartate uptake by Glt_{Ph} is also coupled to co-transport of three sodium ions

[37]. However, transport by Glt_{Ph} is neither coupled to protons nor potassium [38, 32]. Whereas it was clearly demonstrated that Glt_{Ph} mediated transport does not depend on potassium in many publications that followed this was interpreted as Glt_{Ph} does not interact with potassium. However, the idea that Glt_{Ph} might interact with potassium is corroborated by the fact that thallium was used to report on sodium sites in crystallization experiments. Thallium is more similar to potassium than to sodium and it was shown that in EAATs thallium can functionally replace potassium completely but can only partially replace sodium [39].

3.3 K^+ interaction with EAATs

Secondary active transporters couple the uphill transport of one molecule species to the downhill movement of other species. In the most simple case of the coupled transport of two uncharged molecules, transport is maintained as long as the gradient of the second species is larger than that of the transported one. If the transported molecules are ions, we also have to take the charge movement and the membrane voltage into account. In case of the co-transport of n_{Glu} glutamate, n_{Na} sodium and n_{H} hydrogen as well as the counter-transport of n_{K} potassium ions, we obtain

$$\Psi = \frac{RT}{F(n_{\text{Na}} + n_{\text{H}} - n_{\text{K}} - n_{\text{Glu}})} \ln \left(\frac{[\text{Na}]_o^{n_{\text{Na}}} [\text{glu}]_o^{n_{\text{glu}}} [\text{H}]_o^{n_{\text{H}}} [\text{K}]_i^{n_{\text{K}}}}{[\text{Na}]_i [\text{glu}]_i [\text{H}]_i [\text{K}]_o} \right)$$

describing the concentrations at which there is no net flux at a given membrane potential Ψ [7]. Here R denotes the gas constant, F the Faraday constant and T is the absolute temperature. Solving for the glutamate gradient that is maintained yields

$$\frac{[\text{glu}]_i}{[\text{glu}]_o} = \exp \left(\frac{\Psi F (n_{\text{Na}} + n_{\text{H}} - n_{\text{K}} - n_{\text{Glu}})}{RT} \right) \frac{[\text{Na}]_o^{n_{\text{Na}}} [\text{H}]_o^{n_{\text{H}}} [\text{K}]_i^{n_{\text{K}}}}{[\text{Na}]_i [\text{H}]_i [\text{K}]_o}$$

Under physiological conditions EAATs can maintain glutamate concentration gradients larger than 10^6 [7]. The fact that they couple glutamate uptake to three other ion species enables highly concentrative glutamate uptake over a wide range of ionic conditions.

To analyze the contribution of potassium coupling, we rewrite above equation as

$$\frac{[glu]_i}{[glu]_o} = \exp\left(\frac{\Psi F(-n_K)}{RT}\right) \frac{[K]_i^{n_K}}{[K]_o} \exp\left(\frac{\Psi F(n_{Na} + n_H - n_{Glu})}{RT}\right) \frac{[Na]_o^{n_{Na}} [H]_o^{n_H}}{[Na]_i [H]_i}$$

At a membrane voltage of $\Psi = -70\text{mV}$ and a temperature of $T = 310.15\text{K}$ (human body temperature) the first exponential term evaluates to 13.4. Potassium gradients are in the range of 20 [40]. Combining both values, we see that the evolution of the additional coupling to K^+ enables to maintain an almost 300-fold larger glutamate gradient compared to a stoichiometry without potassium. This large gradient allows a better control of the time course of extracellular glutamate concentrations and marks an important step in the evolution of the complex central nervous system.

Furthermore, potassium binding or potassium-bound translocation is believed to be the rate-limiting step in glutamate uptake by EAATs [41]. Therefore it represents a promising pharmacological target to modify EAAT function, not only for activation but also inhibition of EAATs. In ischemic conditions (e.g. after a stroke) oxygen supply and finally the concentration gradients that drive transport break down. The potassium gradient will be the first to decrease because of the high potassium conductance found in cells of the nervous system. Under this conditions extracellular potassium release is slowed down and EAATs will start to work in the reverse direction and transport intracellular glutamate along its concentration gradient out of the cell. The elevated extracellular glutamate levels will lead to additional damage to brain tissue. Some pharmacological agent that selectively prevents extracellular potassium binding to EAATs will stop this process while retaining the glutamate buffering capacity of EAATs. The first step in the development of such an agent is to understand the structural basis of potassium binding to EAATs.

In contrast to glutamate or sodium there is no information from crystal structures regarding potassium. So far there are only indirect results on potassium binding from mutagenesis experiments. A common approach when investigating potassium interaction is to compare results from radioactive uptake experiments under forward transport and glutamate exchange conditions. In mutations that lead to a protein that mediates exchange but not net transport the mutated

residue may interact with potassium. Following this or similar approaches there are several residues that were proposed to be involved in potassium binding [42, 43, 44, 45, 46, 47]. However, when comparing them with the Glt_{Ph} structure those residues cannot belong to one singular binding site. So far there is no conclusion that explains the apparent discrepancy between the findings cited above and the fact that only one potassium is co-transported. What is missing are structural information on potassium binding. Since the Glt_{Ph} has proven to be an excellent model for many aspects of EAATs, we decided to test if we can use Glt_{Ph} also as a model system for K⁺ binding in EAATs.

In this work I used computer simulations of the Glt_{Ph} structure to investigate potassium binding. The results from simulations were then compared with results from whole-cell patch-clamp recordings of mammalian EAAT2.

4. Material and Methods

4.1 MD simulations

All simulations were performed using the GROMACS 5.1.2 [48, 49] software package. The AMBER ff99SB-ILDN force field [50] was used for the protein, Joung parameters for the ions [51], together with the SPC/E water model [52]. The combination of the AMBER force field with SPC/E is supported by a recent force field benchmark [53]. The initial steps for all systems were as follows: First, missing atoms were filled up and mutations introduced during the crystallization procedure were reversed using MODELLER [54]. Then, we modeled additional amino acids resp. removed some to have all structures in the amino acid range from LYS-6 to GLU-416. The protein structures were embedded into a pre-equilibrated POPC bilayer [55] in a box of water and circa 1M KCl, using the *g-membed* methodology [56]. These simulation systems were subjected to several stages of equilibration. In the first stage we applied harmonic position restraints to all protein, non-hydrogen atoms in all three dimensions as well as to the phosphor atoms of the lipids in z-direction. The latter restraints were necessary to avoid any unnecessary perturbation of the lipid bilayer while the system pressure was equilibrating. This first step ran for 4ns and was followed by a second equilibration step in which only the positions restraints of the protein atoms were maintained. This was run until the system density was stable and usually took 500–900ns. In the final equilibration run only the backbone atoms of the protein were restrained, the side-chains were allowed to move freely and from this final 40ns equilibration we took positions and velocities for the production MD runs. Pressure was set to 1bar with a semi-isotropic barostat. For the equilibration the Berendsen barostat [57] was used. In the production runs the Parrinello-Rahman barostat [58] was used. Temperature was set to 310.15K with the velocity-rescale thermostat [59]. Water molecules were constrained with the SETTLE [60] algorithm, while all other bonds were constrained using LINCS [61]. All amino acids were modeled in their default protonation states according to pK_a calculation showing that each titratable residue is most likely in a protonation state corresponding to pH=7 [62]. Long range electrostatic interactions were treated with the particle mesh Ewald (PME) method [63].

From some of those initial MD setups several more runs were spawned to get reasonable statistics for the rates of binding. In this case random velocities were generated for the initial structure and the Berendsen barostat [57] was used. To obtain transition rates between two states, we divided the total number of transitions by the total time spent in the initial state. In all of the unbiased simulations hydrogens were treated as virtual sites and a timestep of 4fs was used [64].

The authors gratefully acknowledges the computing time granted on the supercomputer JURECA [65] at Jülich Supercomputing Centre (JSC).

4.1.1 Free energy calculations

For free energy calculation, snapshots with occupied binding sites were extracted from the free MD trajectories and the salt concentration was reduced to avoid spontaneous binding events in the next steps. The salt concentration was reduced by deleting ions from the structure files, which lead to a decrease in the density of the simulation system. We performed another round of energy minimization and equilibration with position restraints on the protein heavy atoms until all voids were filled and the correct system density was restored. To estimate binding free energies of K^+ binding to WT proteins, we employed umbrella sampling [66] with the distance of a K^+ ion to the binding site in one monomer as reaction coordinate. The reference positions of the binding sites were defined as the centre of mass of three or four C_α atoms. The actual binding sites had distances of around 0.2nm to the reference position. The potential of mean force (PMF) profiles were shifted by this distance such that the first minimum in the PMF is at distance 0. Restraining forces were implemented with the pull-code of GROMACS. First, a bound ion was pulled out of the binding site with a force constant of 1000kJ/mol/nm and a pulling speed of 0.1 nm/ns. From the pulling simulation snapshots at different positions along the reaction coordinate were extracted. Those served as starting structures that were simulated with a restraint potential along the reaction coordinate. Initially we used a 0.05nm spacing of the umbrella windows in the region close the binding site and a 0.1nm spacing for regions far from the binding sites. Force constants between 1000 and 9000 kJ/mol/nm were used starting with high force constants in the region close to the binding site that were decreased along the reaction coordinate. In cases of

large barriers in the PMF which are indicated by poor overlap of histograms of adjacent windows or by histograms with more than one peak, we added more windows with smaller spacing and larger force constants. To obtain a well-sampled end state where the ion is in bulk solution, and especially to avoid interaction of the ion with the other monomers, we also applied a flat-bottom potential in the xy-plane. This flat bottom potential acted at distances larger than 1.3nm and had a force constant of 1500kJ/mol/nm. Data were unbiased with the weighted histogram method (WHAM) [67] as implemented in the GROMACS module *gmx wham* [68]. The standard free energy of binding and equilibrium constants were calculated from the PMF as described in [69]. The dissociation constant K_D is decomposed into a product

$$K_D^{-1} = S \cdot I$$

where I is the integral of the PMF $W(r)$ in the binding site

$$I = \int_{\text{site}} \exp(-(W(r) - W(r_b)/RT)) dr$$

where r describes the reaction coordinate, i.e. the distance between an ion and the binding site. r_b is a reference position in the bulk solution, here $r_b = 4.0\text{nm}$. The binding site was defined to range from the first minimum in the PMF to a distance of 0.4nm from the first minimum. The term S denotes the surface area that is sampled by the ligand at distance r_b from the binding site [69]. In our case this is given as the fraction of the surface of a sphere with radius r_b that is cut out by the flat-bottom restraining cylinder of radius $r_0 = 1.3\text{nm}$.

$$S = \pi \left(r_0^2 + \left(r_b - \sqrt{r_b^2 - r_0^2} \right)^2 \right)$$

In all of the umbrella sampling simulations hydrogens were treated as virtual sites and a timestep of 4fs was used [64].

To investigate the effect of mutations in the protein on K^+ binding, we calculated the change in free energy when alchemically transforming one amino acid side-chain into another in a K^+ bound monomer. In the case of an Asp to Asn mutation this would introduce a net charge in the system which would introduce artifacts when using the PME [70]. To avoid this problem, we made use of the

trimeric structure of Glt_{Ph} and performed the reverse mutation in another K⁺ free monomer. First, the mutation was introduced into one K⁺ free monomer with the PyMOL mutagenesis wizard. Then topologies for alchemical transformations were set up using the *pmx* package [71]. The end states were: 1. wild-type side-chain in a K⁺ bound monomer and mutated side-chain in a K⁺ free monomer. 2. mutated side-chain in K⁺ bound monomer and wild-type side-chain in K⁺ free monomer. From long simulations of those end states, 160 frames were extracted and used as starting structures for fast growth runs in which the side-chain is alchemically transformed within 5 or 10ns. The resulting work distributions were analyzed with the Crooks Gaussian intersection method [72] as implemented in the *pmx* package. This method is based on Crooks fluctuation theorem [73]

$$\frac{P_f(W)}{P_b(-W)} = \exp((W - \Delta G)/RT)$$

where P_f resp P_b denote the work distributions of the forward resp. backward transition. From this equation it readily follows that ΔG is given by the intersection point of both distributions.

For a complete thermodynamic cycle the same protocol was applied to a system where both monomers are K⁺ free. Since the alchemical transformation also affected hydrogens, those were not modeled as virtual sites and a timestep of 2fs was used.

4.1.2 Gating charge calculations

Gating charges, i.e. the net charge transfer across the membrane associated with K⁺ binding, were calculated using the method developed by Machtens et al. [74]. Briefly, computational electrophysiology simulations in GROMACS [75] were used to simulate Glt_{Ph} under various electrochemical potential gradients to infer gating charges from the $\Delta q - V$ relationship for Glt_{Ph} in different states. To this end, anti-parallel double-bilayer systems were set up with the protein restrained to one conformation. These systems were then simulated under different ionic charge imbalances, resulting from small ionic number differences between the two aqueous compartments, and the resulting transmembrane voltage was calculated from the charge densities using Poisson's equation. In such a setup

the membrane voltage V is given by

$$V = \frac{q}{C_0} = \frac{q_{sol} + q_{p0}}{C_0}$$

where q_{sol} represents the ionic charge imbalance in the aqueous compartment and q_{p0} is the contribution of the protein in state 0; C_0 is the total membrane/protein capacitance. The voltage in the system is measured for different values of q_{sol} and q_{p0} is inferred by linear regression. This procedure is performed for different states of the protein and the charge movement associated to a transition between states 0 and 1 is calculated via

$$Q_{01} = q_{p0} - q_{p1}$$

4.2 Experimental

4.2.1 Whole-cell patch-clamp

The standard bath solution for all patch-clamp experiments contained (in mM) 140 NaNO₃, 1 MgCl₂, 2 CaCl₂, 5 TEA-Cl, 10 HEPES, and pH 7.4 adjusted with NMDG. For some experiments 5mM Glu was added to the standard solution or NaNO₃ was equimolarly substituted by KNO₃ or CholineNO₃. Pipette solution contained either (in mM) 115 KNO₃, 2 MgCl₂, 5 EGTA, 10 HEPES, and pH 7.4 adjusted with KOH; or 115 NaNO₃, 5 Glu, 2 MgCl₂, 5 EGTA, 10 HEPES, and pH 7.4 adjusted with NaOH. HEK293T cells were transiently transfected with calcium phosphate as described in [76] with volumina scaled down by a factor of 1/3 for the use in 5cm dishes and 1μg of DNA per transfection was used. Cells were splitted 20–24h after transfection and measured 20–28h after splitting. Before patch-clamp experiments, cells were washed twice with standard bath solution and also kept in standard bath solution. Currents were recorded using a HEKA EPC10 amplifier (HEKA Elektronik Dr. Schulze GmbH, Wiesenstraße 71, 67466 Lambrecht/Pfalz), filtered at 10kHz and sampled at 50kHz. Different extracellular conditions were applied by moving the cell into streams of different solution that were applied by a self-made gravity-driven perfusion system. We applied voltage jumps to in a range between -170 and +135 mV, cells were held at 0mV for 4s between sweeps.

Fast solution exchange was performed as described in [77] with a MXPZT-300L piezo device (Siskiyou Corporation, 110 SW Booth Street, Grants Pass, OR 97526). The kinetics of the solution exchange were measured after each experiment by blowing of the cell and measuring the time course of the open tip response. Rise-times (10%–90%) of the open tip response were in the range of 1ms.

4.2.2 Microscale thermophoresis

We performed microscale thermophoresis (MST) experiments [78] to test ion binding to Glt_{Ph}. Purified and solubilized Glt_{Ph} was labelled with the dye NT-495 (NanoTemper Technologies GmbH, Flößergasse 4, 81369 München), and a series of buffers containing a constant amount of Glt_{Ph} protein and different Na⁺ resp. K⁺ concentrations in the range of 0.6 to 1500mM was prepared. Molarity was kept constant in all buffers by substitution of Na⁺ with choline. Each buffer was exposed to a temperature jump and the change in fluorescence in the heated volume was recorded over time using a Monolith NT.115 (NanoTemper Technologies GmbH, Flößergasse 4, 81369 München) instrument. The steady state fluorescence after the temperature jump was plotted vs. the ligand concentration to obtain a binding curve. Upon the temperature jump the fluorescence rapidly decreases, which is a property of the dye and does not report on thermophoresis. Therefore, the steady state fluorescence was normalized to the value measured 0.4s after the temperature jump.

4.3 Data analysis

Simulation data were analyzed with a combination of GROMACS tools and self-written python scripts except for the alchemical transformations, which were analyzed with the *pmx* package [72]. Experimental data were analyzed with a combination of FitMaster (HEKA Elektronik Dr. Schulze GmbH, Wiesenstraße 71, 67466 Lambrecht/Pfalz) and self-written python scripts. I–V curves were generated by plotting the average normalized current amplitudes at the end of a voltage jump versus the applied voltage. To analyze the K⁺ dependence of anion currents, steady-state currents at -170mV were measured at different K⁺ concentrations, where choline was used to keep the molarity constant. First, data

from each cell was normalized to the maximum current from fitted Hill functions. For the concentration-response plot these normalized currents were averaged and plotted vs. the extracellular K^+ concentration. Parameter estimates are means from bootstrap sampling of the pooled normalized current data. Error bars of anion currents are SD of normalized currents from independent experiments. Errors of fit parameters or parameters estimated from MD data are SD from bootstrap sampling [79]. In case of umbrella sampling, bootstrap sampling was performed using the trajectory method implemented in *gmx wham* [68], i.e. for each umbrella window new trajectories were bootstrapped from the original ones and then fed into the wham algorithm. In case of composed quantities, we used standard propagation of error formulas [80]. Plots were also prepared with python scripts. Figures of protein structures were generated using PyMOL [81].

5. Results

5.1 MD simulations of Glt_{Ph} reveal three binding sites

To investigate K⁺ binding, we set up MD systems based on different crystal structures of Glt_{Ph}. In our simulation all bound substrates were removed from the coordinate files. The starting conformations and the removed ligands of the different structures are summarized in Table 5.1. The structures were then embedded in a POPC bilayer and solvated in a water box with a concentration of circa 1M KCl in the bulk solution. In this step we also included one structure of another EAAT homolog Glt_{Tk} [82].

MD no.	PDB ID	conformation	removed substrates	time (μ s)	remarks
MD1	2NWW	outward-facing, HP open	Na ⁺ + TBOA	2.7	K1,K3 binding
MD2	2NWX	outward-facing, HP closed	2Na ⁺ + Glutamate	1.6	K1,K2,K3 binding
MD3	4OYE	outward-facing, HP closed	apo	1.4	K3 binding
MD4	4OYF	outward-facing, HP closed	Na ⁺	1.01	K1,K2,K3 binding
MD5	4KY0	outward-facing, HP closed	apo	1.4	K2,K3 binding
MD6	3KBC	inward-facing, HP closed	2Na ⁺ + Glutamate	2.2	K1,K2,K3 binding

Table 5.1: Initial MD setups. *Conditions used to test for spontaneous K⁺ binding.*

5.1.1 Spontaneous binding events in free MD

We subjected each of these systems to at least 1 μ s of free MD simulations and checked for K⁺ binding. We found that K⁺ ions bind to three distinct sites in unbiased MD simulations of outward-facing conformations (Figure 5.1).

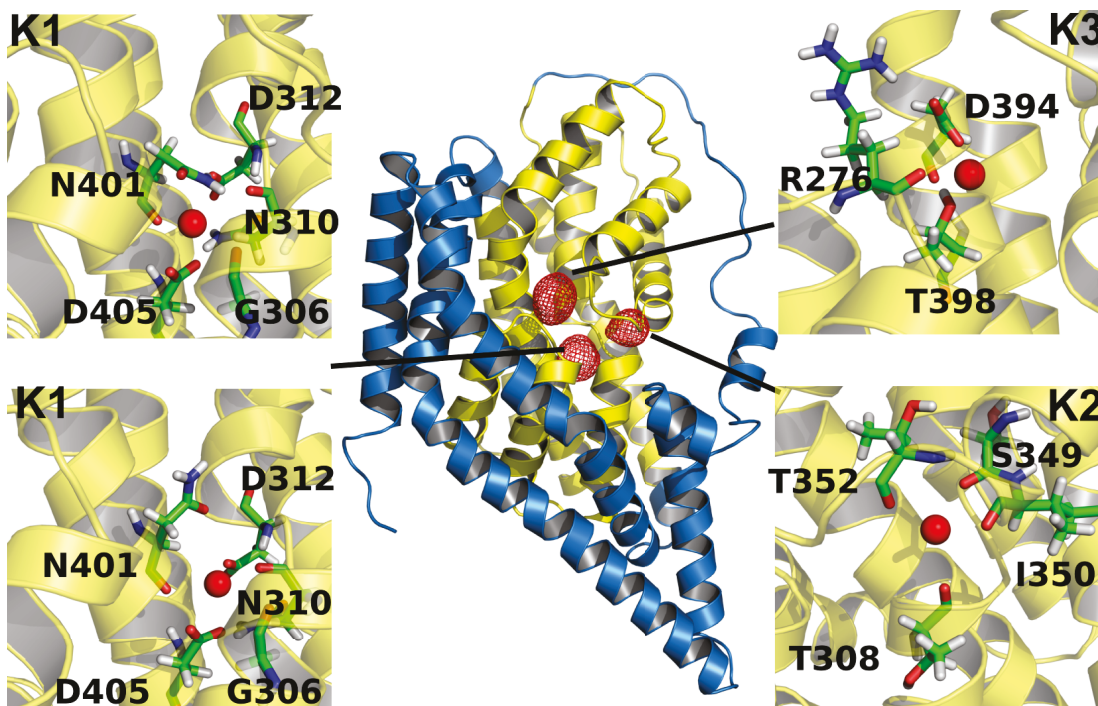


Figure 5.1: Representative spontaneous binding in MD. *Result from a simulation of outward-facing Glt_{Ph} structure (MD_4) representing all observed binding sites in MD. The mesh indicates regions with high potassium density inside the transport-domain contoured at 1.5σ . The density was calculated from pooled data of all three monomers. Close-ups show a bound K^+ ion in the binding site (red sphere) and stick representations of binding site forming residues.*

The first site, denoted as K1 in the following, overlaps partly with the known Na1 and the Na3 [36] sites and is also similar to a site that was identified in an EAAT3 homology model and named K^+ site1 by Heinzelmann et al. [83]. The ligating atoms are the main-chain oxygens of residues G306, N310 and N401 as well as the side-chain oxygens of N310, D312, N401, and D405. It shares the main-chain oxygen of N401, the main-chain oxygen of N310 and the side-chain oxygens of D405 with the Na1 site, whereas the side-chains of G306 and S278 that are also part of the Na1 site are not involved in coordinating a K^+ ion at this site. A common interaction with the Na3 site is the side-chain oxygen of D312. We found the K1 site in two different conformations. In the first conformation the side-chain of N401 is coordinating a bound K^+ ion, whereas the side-chain of D312 is not involved (Figure 5.1, K1 site top panel). In the second conformation the

ion moves closer to TM7 and the side-chain of N401 flips away, so that the D312 side-chain ligates the K^+ ion (Figure 5.1, K1 bottom). The second site, which we denote as K2, is identical to the known Na2 site [32]. The ligating atoms are the main-chain oxygens of residues T308, S349, I350, and T352 (Figure 5.1, K2 panel). The third site, which we denote as K3, was already suggested by Holley et al. [84]. It was named Ct site by Verdon et al. and has been speculated to be a K^+ binding site in EAATs [31]. A K^+ ion at this site is coordinated by the side-chain oxygens of D394 and T398 and the main-chain oxygen of R276 (Figure 5.1, K3 panel). Table 5.2 shows homologous residues in the EAATs according to the alignment in [11]. Notably almost all the residues are conserved between Glt_{Ph} and all EAAT isoforms. Especially all residues that contribute side-chain atoms to ion coordination are completely conserved in all EAAT isoforms.

Glt_{Ph}	EAAT1	EAAT2	EAAT3	EAAT4	EAAT5
G306	G394	G393	G362	G416	G373
T308	T396	T395	T364	T418	T375
N310	N398	N397	N366	N420	N377
D312	D400	D399	D368	D422	D379
S349	S436	S435	S404	S458	S415
I350	I437	V436	I405	V459	I416
T352	A439	A438	A407	A461	A419
D394	D476	D475	D444	D498	D456
T398	T480	T479	T448	T502	T459
N401	N483	N482	N451	N505	N462
D405	D487	D486	D455	D509	D466

Table 5.2: Alignment of binding site forming residues. *Ligating residues found in MD and their homologous EAAT residues. Residues that contribute side-chain atoms are marked in boldface.*

We did not observe unbinding from the K1 site in any of the simulations performed so far suggesting that K1 is the most stable site. However, we see several binding and unbinding events at the K2 and K3 sites. We therefore speculate that the K1 site has the highest affinity for K^+ and that it is the site which is occupied during the transition between inward- and outward-facing

states of the transport domain.

Simulations with other conformations of Glt_{Ph} revealed the same sites also in these simulations. Figure 5.2 and Table 5.1 show an overview of the results of the simulations with the other structures.

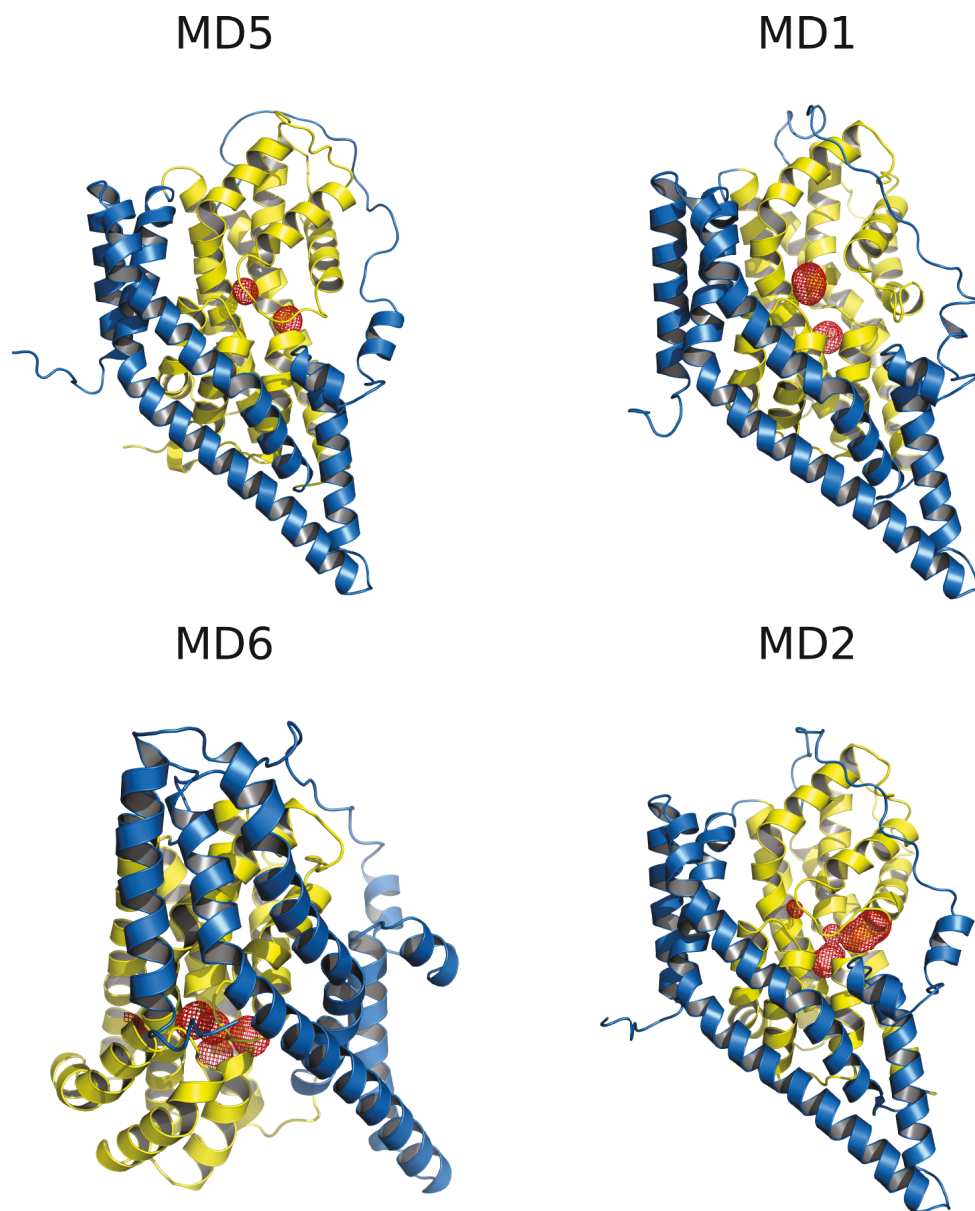


Figure 5.2: Overview of spontaneous binding events. *Results from different conformations. The meshes indicate regions with high potassium density inside the transport-domain contoured at 1.5σ .*

When inspecting individual binding trajectories we observed multiple binding patterns. For outward-facing structures we observed two pathways: (1) A K^+ ion binds to K3, followed by the binding of another one to K1. (2) K^+ binds initially to K2 and then hops to K1. Figure 5.3 shows representative trajectories for each binding pathway.

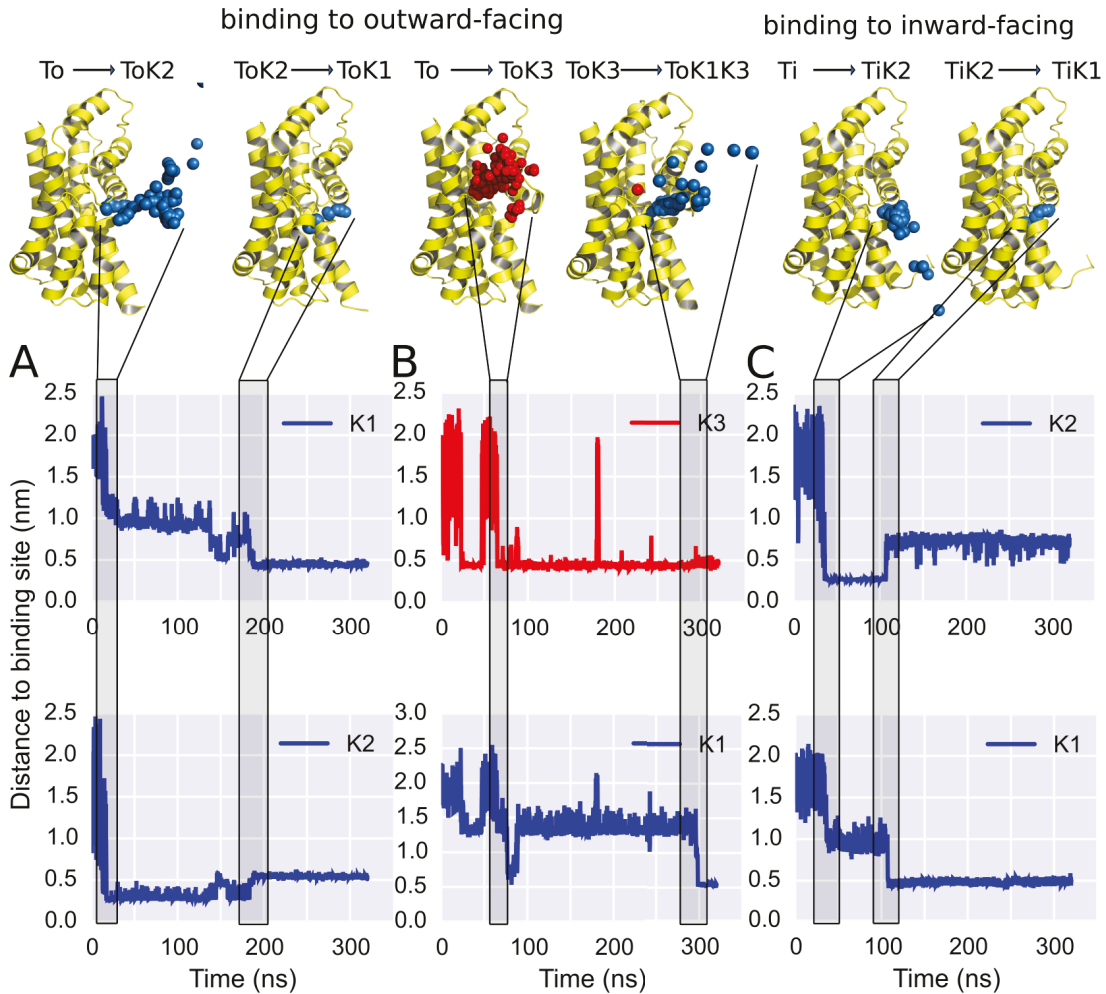


Figure 5.3: Representative trajectories of binding events. *The spheres represent snapshots of a K^+ ion on its way to the binding site. Plots show the time evolution of the distance of the closest K^+ to the binding sites. A, First, a K^+ binds to K2, then the same ion hops to K1. B, K3 gets occupied first (colored red), then another K^+ (blue) binds to K1. C, In the inward-facing conformation only hopping via K2 is observed.*

In outward-facing states of the transporter the K3 and K2 sites are accessible from the bulk solution and are occupied first. In the first pathway binding of K3 is coupled to slight opening of HP2 which opens a way for the second K^+ that will bind at K1. In case of the second pathway no movement of the hairpin gate is necessary, an ion at K2 can readily hop to K1 without further rearrangements in the protein conformation.

In the simulation of the inward-facing conformation only the latter pathway was observed when analyzing K1 binding (Figure 5.3 C). We also see binding to K3 in inward-facing conformation but it is not coupled to binding at K1. One major difference between inward- and outward-conformations is that the binding sites are not accessible from bulk solution directly. The ions have to travel via a volume that is constrained by HP1, TM7 and TM5.

So far we identified three potential binding sites and found distinct contributions of K1, K2 and K3 to K^+ binding. However, all of our observations are based on a small number of events and do not allow for a quantitative analysis. For this reason we performed more simulations with an inward-facing (MD6) as well as with an outward-facing structure (MD2).

5.1.2 Extensive parallel MD simulations allow estimation of kinetic parameters

In single long simulation trajectories there are only few binding events so that we get only inaccurate estimates for kinetic parameters. To improve statistics and to test the hypothesis that there are two pathways to K1 binding, we took the initial frames of previous MD simulations and started a set of 65 simulations in parallel each with different initial velocities. It is more efficient to produce several short trajectories since MD simulations only moderately scale with the number of processors used. Kinetic parameters for K^+ binding are estimated as described in Figure 5.4.

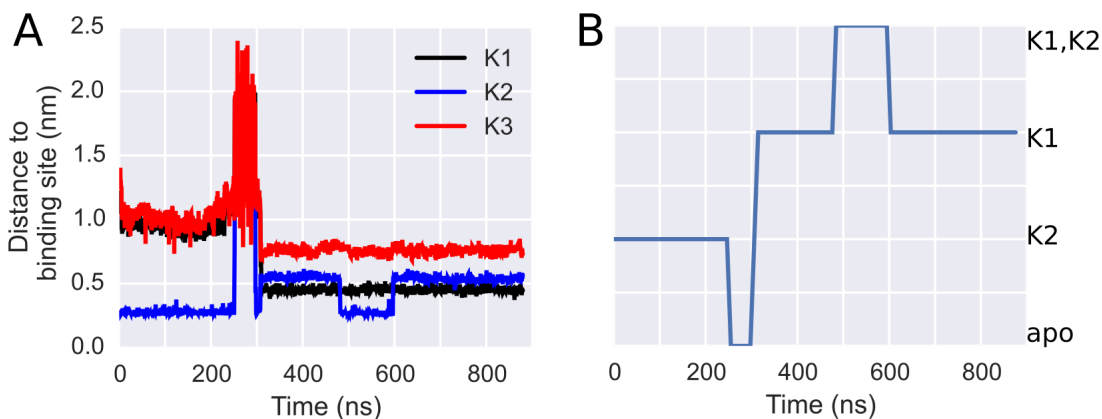


Figure 5.4: Counting transitions between binding sites. *Raw distance data from MD simulations is sorted into a set of discrete states. A, Time evolution of the distance of the closest K^+ to the binding sites. B, The data from A is sorted into discrete states.*

For each simulation and each monomer the distance of K^+ ions to the binding sites is measured and each frame is associated with a bound state according to its distance. The distance thresholds that define the bound state were 0.5nm for K2 and 0.7nm for K1 and K3. The rates between two states 0 and 1 are estimated via

$$k_{01} = \frac{N_{01}}{t_0}$$

where N_{01} is the number of transitions from state 0 to state 1 and t_0 is the time spent in 0. The rates can then be used to calculate equilibrium constants between states.

$$K_{eq} = \frac{k_{01}}{k_{10}}$$

The raw data were manually refined because some hopping events from K2 to K1 were falsely identified as unbinding from K2 to bulk before binding to K1. We also found some events, in which an ion moves away from K1 beyond the threshold that was used to define the bound state, but the very same ion quickly moves back into the binding sites. Those were not counted as unbinding events. The full results of this analysis are summarized in Tables 5.3–5.10. Figure 5.5 shows a condensed state diagram of the transition that lead to K1 occupation.

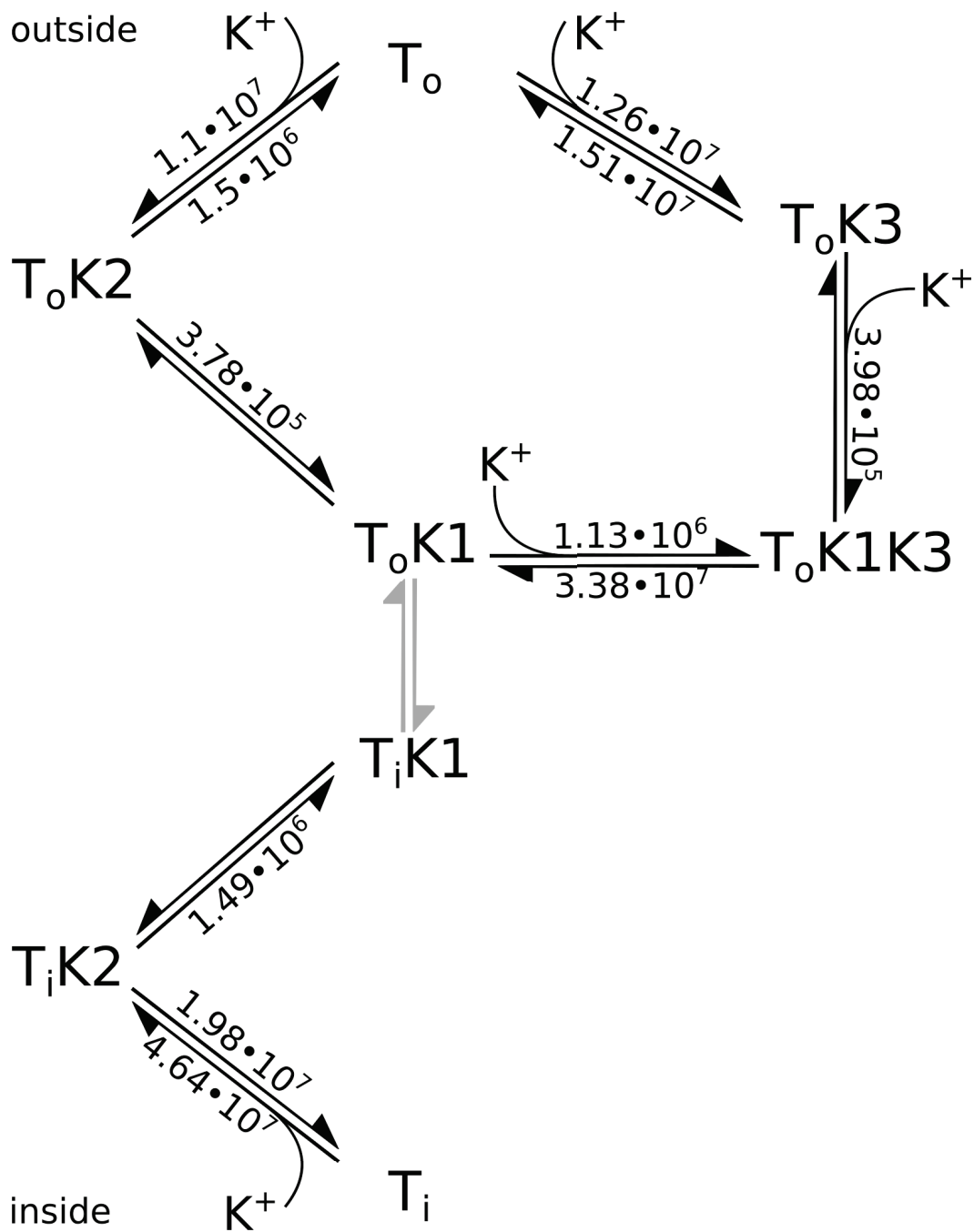


Figure 5.5: State diagram for K1 binding. A kinetic scheme with calculated rates (s^{-1}) for the binding pathways that lead to K1 binding.

	apo	K3	K2	K2K3	K1	K1K3	K1K2	K1K2K3
apo	556275	147	1295	0	0	0	0	0
K3	135	111241	4	355	1	0	0	0
K2	1207	5	1217096	91	91	0	0	0
K2K3	0	356	82	87475	0	0	0	0
K1	0	0	0	0	652723	3	332	0
K1K3	0	0	0	0	3	228	0	0
K1K2	0	0	0	0	300	0	410614	0
K1K2K3	0	0	0	0	0	0	0	0

Table 5.3: Number of transitions, inward-facing. *Observed number of transitions between states, inward-facing*

	apo	K3	K2	K3K2	K1	K1K3	K1K2	K1K2K3
total	$3.07 \cdot 10^{-5}$	$5.70 \cdot 10^{-6}$	$5.98 \cdot 10^{-5}$	$4.89 \cdot 10^{-6}$	$3.67 \cdot 10^{-5}$	$3.27 \cdot 10^{-8}$	$1.64 \cdot 10^{-5}$	0.0
relative	18.3	3.7	40.1	2.9	21.5	0.007	13.5	0.0

Table 5.4: Times spent in states, inward-facing. *Absolute time(s) and relative time(%) in states, inward-facing*

	apo	K3	K2	K2K3	K1	K1K3	K1K2	K1K2K3
apo	$1.99 \cdot 10^{10}$	$5.27 \cdot 10^6$	$4.64 \cdot 10^7$	0	0	0	0	0
K3	$2.42 \cdot 10^7$	$1.99 \cdot 10^{10}$	$7.16 \cdot 10^5$	$6.35 \cdot 10^7$	$1.79 \cdot 10^5$	0	0	0
K2	$1.98 \cdot 10^7$	$8.21 \cdot 10^4$	$2.00 \cdot 10^{10}$	$1.49 \cdot 10^6$	$1.49 \cdot 10^6$	0	0	0
K2K3	0	$8.10 \cdot 10^7$	$1.87 \cdot 10^7$	$1.99 \cdot 10^{10}$	0	0	0	0
K1	0	0	0	0	$2.00 \cdot 10^{10}$	$9.19 \cdot 10^4$	$1.02 \cdot 10^7$	0
K1K3	0	0	0	0	$2.55 \cdot 10^8$	$1.94 \cdot 10^{10}$	0	0
K1K2	0	0	0	0	$1.46 \cdot 10^7$	0	$2.00 \cdot 10^{10}$	0
K1K2K3	0	0	0	0	0	0	0	0

Table 5.5: Transition rates, inward-facing. *Transition rates (s^{-1}) between states, inward-facing*

	apo	K3	K2	K2K3	K1	K1K3	K1K2	K1K2K3
apo	1.00	$4.58 \cdot 10^0$	$4.27 \cdot 10^{-1}$	0	0	0	0	0
K3	$2.18 \cdot 10^{-1}$	1.00	$1.15 \cdot 10^{-1}$	1.27	0	0	0	0
K2	2.34	8.72	1.00	$1.25 \cdot 10^1$	0	0	0	0
K2K3	0	$7.85 \cdot 10^{-1}$	$8.01 \cdot 10^{-2}$	1.0	0	0	0	0
K1	0	0	0	0	1.00	$2.78 \cdot 10^3$	1.44	0
K1K3	0	0	0	0	$3.60 \cdot 10^{-4}$	1.0	0	0
K1K2	0	0	0	0	$6.96 \cdot 10^{-1}$	0	1.0	0
K1K2K3	0	0	0	0	0	0	0	0

Table 5.6: Equilibrium constants, inward-facing. *Equilibrium constants between states, inward-facing*

	apo	K3	K2	K2K3	K1	K1K3	K1K2	K1K2K3
apo	348253	219	191	0	0	0	0	0
K3	189	250806	0	87	0	5	0	0
K2	139	0	1849518	168	35	0	0	0
K2K3	0	90	148	153174	0	0	0	2
K1	0	0	0	0	282468	16	22	0
K1K3	0	0	0	0	22	13001	0	3
K1K2	0	0	0	0	13	0	60082	10
K1K2K3	0	0	0	0	0	4	9	7063

Table 5.7: Number of transitions, outward-facing. *Number of transitions between states, outward-facing*

apo	K3	K2	K3K2	K1	K1K3	K1K2	K1K2K3
$1.74 \cdot 10^{-5}$	$1.26 \cdot 10^{-5}$	$9.25 \cdot 10^{-5}$	$7.67 \cdot 10^{-6}$	$1.41 \cdot 10^{-5}$	$6.51 \cdot 10^{-7}$	$3.01 \cdot 10^{-6}$	$3.54 \cdot 10^{-7}$
11.8	8.5	62.4	5.2	9.5	0.4	2.0	0.2

Table 5.8: Times spent in states, outward-facing. *Absolute time(s) and relative time(%) in states, outward-facing*

	apo	K3	K2	K2K3	K1	K1K3	K1K2	K1K2K3
apo	$2.00 \cdot 10^{10}$	$1.26 \cdot 10^7$	$1.10 \cdot 10^7$	0	0	0	0	0
K3	$1.51 \cdot 10^7$	$2.00 \cdot 10^{10}$	0	$6.93 \cdot 10^6$	0	$3.98 \cdot 10^5$	0	0
K2	$1.50 \cdot 10^6$	0	$2.00 \cdot 10^{10}$	$1.82 \cdot 10^6$	$3.78 \cdot 10^5$	0	0	0
K2K3	0	$1.17 \cdot 10^7$	$1.93 \cdot 10^7$	$2.00 \cdot 10^{10}$	0	0	0	$2.61 \cdot 10^5$
K1	0	0	0	0	$2.00 \cdot 10^{10}$	$1.13 \cdot 10^6$	$1.56 \cdot 10^6$	0
K1K3	0	0	0	0	$3.38 \cdot 10^7$	$2.00 \cdot 10^{10}$	0	$4.61 \cdot 10^6$
K1K2	0	0	0	0	$4.33 \cdot 10^6$	0	$2.00 \cdot 10^{10}$	$3.33 \cdot 10^6$
K1K2K3	0	0	0	0	0	$1.13 \cdot 10^7$	$2.54 \cdot 10^7$	$2.00 \cdot 10^{10}$

Table 5.9: Transition rates, outward-facing. *Transition rates (s^{-1}) between states, outward-facing*

	apo	K3	K2	K2K3	K1	K1K3	K1K2	K1K2K3
apo	1.00	1.20	$1.37 \cdot 10^{-1}$	0	0	0	0	0
K3	$8.34 \cdot 10^{-1}$	1.00	0	1.69	0	0	0	0
K2	7.29	0	1.00	$1.06 \cdot 10^1$	0	0	0	0
K2K3	0	$5.91 \cdot 10^{-1}$	$9.41 \cdot 10^{-2}$	1.00	0	0	0	0
K1	0	0	0	0	1.00	$2.98 \cdot 10^1$	2.78	0
K1K3	0	0	0	0	$3.35 \cdot 10^{-2}$	1.00	0	2.45
K1K2	0	0	0	0	$3.60 \cdot 10^{-1}$	0	1.00	7.65
K1K2K3	0	0	0	0	0	$4.07 \cdot 10^{-1}$	$1.31 \cdot 10^{-1}$	1.00

Table 5.10: Equilibrium constants, outward-facing. *Equilibrium constants between states, outward-facing*

In total we observed 92 binding events to K1 in inward-facing conformations, 91 were first binding to K2 then hopping to K1. In one case we observed hopping from K3 to K1. For the outward-facing conformation we observed 40 binding events at K1, 35 were hopping from K2 and 5 were binding of an K^+ from solution while K3 was bound. Several binding and unbinding events at the K2 and K3 site permit calculation of affinities for those sites. In particular we can calculate the effect of K1 binding on the other two sites. For the outward-facing conformation, we calculate a dissociation constant of $0.14M$ for K2 before K1 binding, and $2.8M$ when K1 is bound. For K3 we have $1.2M$ before and $29M$ when K1 is occupied. The inward-facing conformation shows the same behavior: We calculated the affinity of K2 binding as $0.4M$ before and $1.4M$ after K1 binding. For K3 the result is a dissociation constant of $4.5M$ before K1 binding and $2.78 \cdot 10^3M$ after.

For K1 these simulations showed the same pattern as before: Once a K^+ ion has bound in K1, it does not leave within the simulation. This is a strong indicator for a high affinity for K^+ at the K1 site but prevents estimation of the K1 affinity since the off-rate cannot be quantified; at least not without making additional assumptions. To get at least a rough estimate, one can consider the probability to observe n events in time t with rate k , which is Poisson-distributed:

$$P(n) = \frac{(kt)^n}{n!} \exp(-kt)$$

For $n = 0$ we get

$$P(0) = \exp(-kt)$$

Taking the logarithm and dividing by $-t$ yields

$$k = -\frac{\log(P(0))}{t}$$

For the outward-facing state the time spent in K1 bound states is $t = 1.41 \cdot 10^{-5}s$ (Table 5.8). If we assume that we did not observe a unlikely event and arbitrarily choose $P(0) = 0.5$, we end up with an unbinding rate at K1 of $49159s^{-1}$. With an rate for hopping from K2 to K1 of $3.78 \cdot 10^5s^{-1}$ (Table 5.9) the equilibrium constant between K2 and K1 is in the range of 0.13. So K1 has indeed a larger affinity for K^+ than K2 and K3. The same procedure with the results from inward-facing states gives an equilibrium constant between K2 and K1 bound states of 0.013. So K1 has the highest affinity in both conformations. In inward-facing states the equilibrium between K1 and K2 is shifted more to K1 than in outward-facing states. And even after taking the different affinities for K2 into account we can conclude that binding to K1 is more favorable in inward- than in outward-facing conformations (Table 5.11). All the values presented here depend on the initial choice of $P(0) = 0.5$. However, the qualitative results presented here do not strongly depend on this value. Assuming that the affinity for K1 is not larger than that of K2, i.e. the unbinding rate is not faster than the binding rate of $3.78 \cdot 10^5s^{-1}$, and calculating the probability to observe no binding events gives $P(0) < 0.005$. Hence the affinity of K1 is significantly larger than that of K2.

conformation	K1	K2	K3
outward-facing	0.007	0.14	1.2
inward-facing	0.005	0.43	4.6

Table 5.11: K_D from free MD (M). Values for $K2$ and $K3$ are taken from Tables 5.10 and 5.6. The values for $K1$ are estimated by multiplying the value calculated above with the affinity of $K2$.

The values in Tables 5.4 and 5.8 do not represent equilibrium values and have to be interpreted with care. The values for $K2$ and $K3$ are artificially large because this state is at the beginning of the process of $K1$ binding. However, when comparing the values for inward- and outward-facing conformations they further corroborate that $K3$ is not involved in K^+ binding from the inside. Moreover it is indicated that a state with all three sites occupied is very unlikely for both inward- as well as outward-facing conformations.

The parallel simulations confirmed the existence of two pathways leading to $K1$ binding that involve either $K2$ and $K3$ and they enable us to calculate kinetic parameters for $K2$ and $K3$. The parameters obtained for $K2$ and $K3$ binding before and after $K1$ binding indicate that $K2$ and $K3$ are only transient sites. Furthermore the binding pathway via $K3$ is only seen in outward-facing states and is the less likely pathway in outward-facing simulations. To overcome the problem of no unbinding at $K1$, we started another set of simulations in which we performed umbrella sampling to calculate the free energy of binding for the different binding sites. The combination of both results allowed a reliable estimate of on- as well as off-rates for all the binding sites.

5.1.3 Free energy of K^+ binding by Umbrella sampling

To determine binding affinities for all three sites, we performed umbrella sampling simulations that enable to get insights into regions of a reaction coordinate that are only rarely sampled in conventional MD. Figure 5.6 describes the idea behind umbrella sampling.

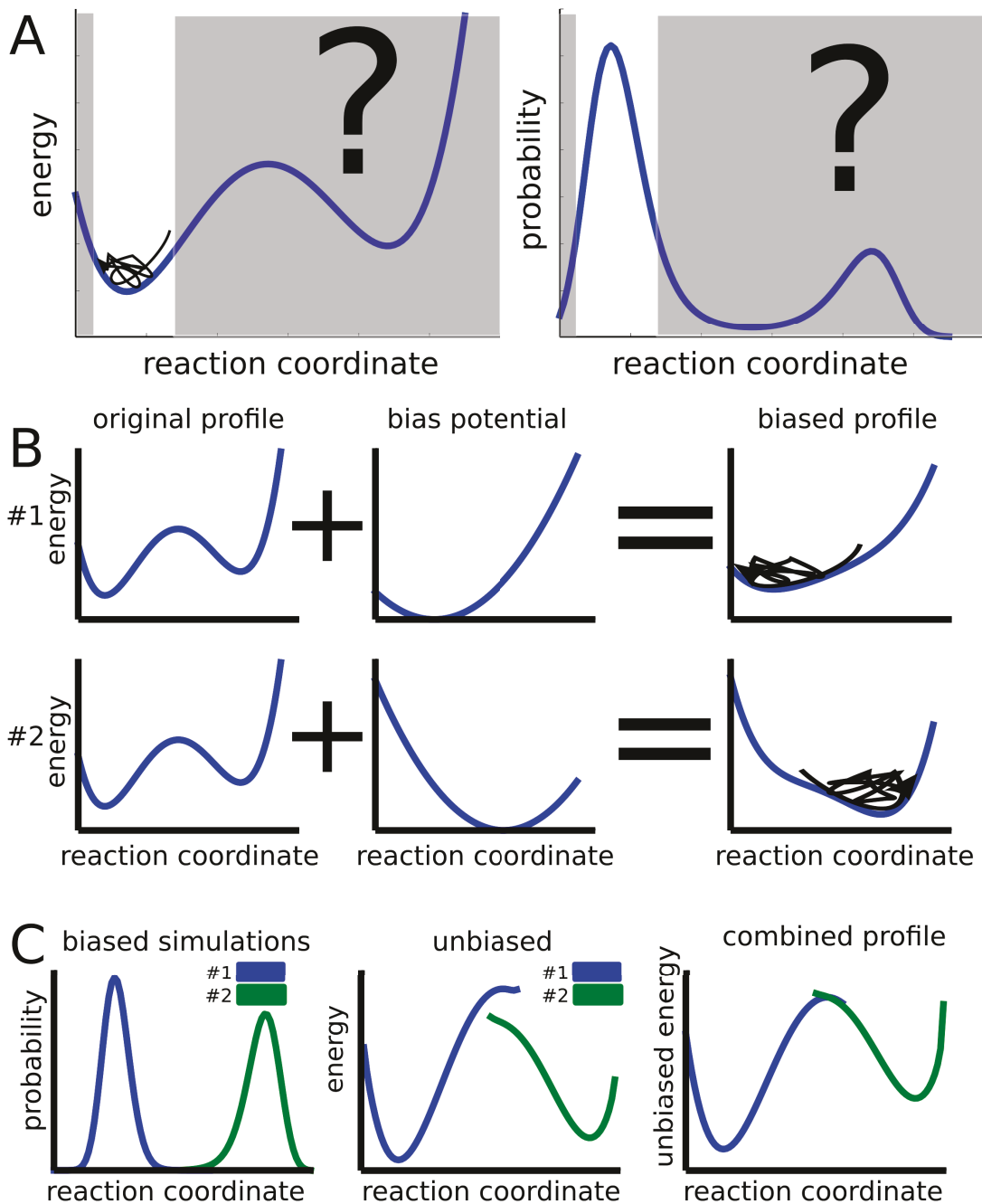


Figure 5.6: Principles of the umbrella sampling method. *A*, If the system gets trapped in a local minimum of the free energy surface, no information about the surface outside this minimum is gained. *B*, Adding different bias potentials, forces the system to sample regions outside the minimum. *C*, With the known bias the original energy profile is reconstructed locally and the outcomes of several simulations is combined to get the global unbiased profile.

In an unbiased simulation the system may get trapped in a local minimum of the potential energy (Figure 5.6 A) and little information about the systems energy outside this minimum is gained. This is what happened in our simulation with the K1 site. To solve this problem, one could simulate for longer times, but we already saw in the last section that we would probably need prohibitively expensive simulations. Instead of waiting for the system to sample all relevant regions, the system is forced to sample certain regions by an additional external bias potential that is added to the force field. With the added bias, a different region of the reaction coordinate is sampled (Figure 5.6 B). Since the bias is known, the unbiased profile can be reconstructed. This procedure is performed for a series of bias potentials each yielding local estimates of the original energy profiles around the restrained position. The local results are combined to give the global unbiased profile (Figure 5.6 C).

We performed umbrella sampling for all three binding sites in the outward- as well as in the inward-facing closed structures. We chose the distance from a K^+ ion to the binding site in all three dimensions as the reaction coordinate. This distance was restrained with harmonic bias potentials. To get snapshots along the reaction coordinate, a bound ion is pulled away from the binding site before starting the actual umbrella sampling simulations. Those are then used as starting points for the umbrella simulations with the distances of the ion to the binding site restrained with a harmonic bias potential. Figure 5.7 shows the resulting PMF profiles. The first minimum corresponds to the bound state and the flat region at large distance corresponds to the unbound state where the ion is in bulk solution and not interacting with the protein. Values of the free energy of binding and dissociation constants after removing the bias of the restraining potentials are given in Tables 5.13 and 5.12. The relation of ΔG and K_D is given by

$$K_D = \exp(\Delta G/RT)$$

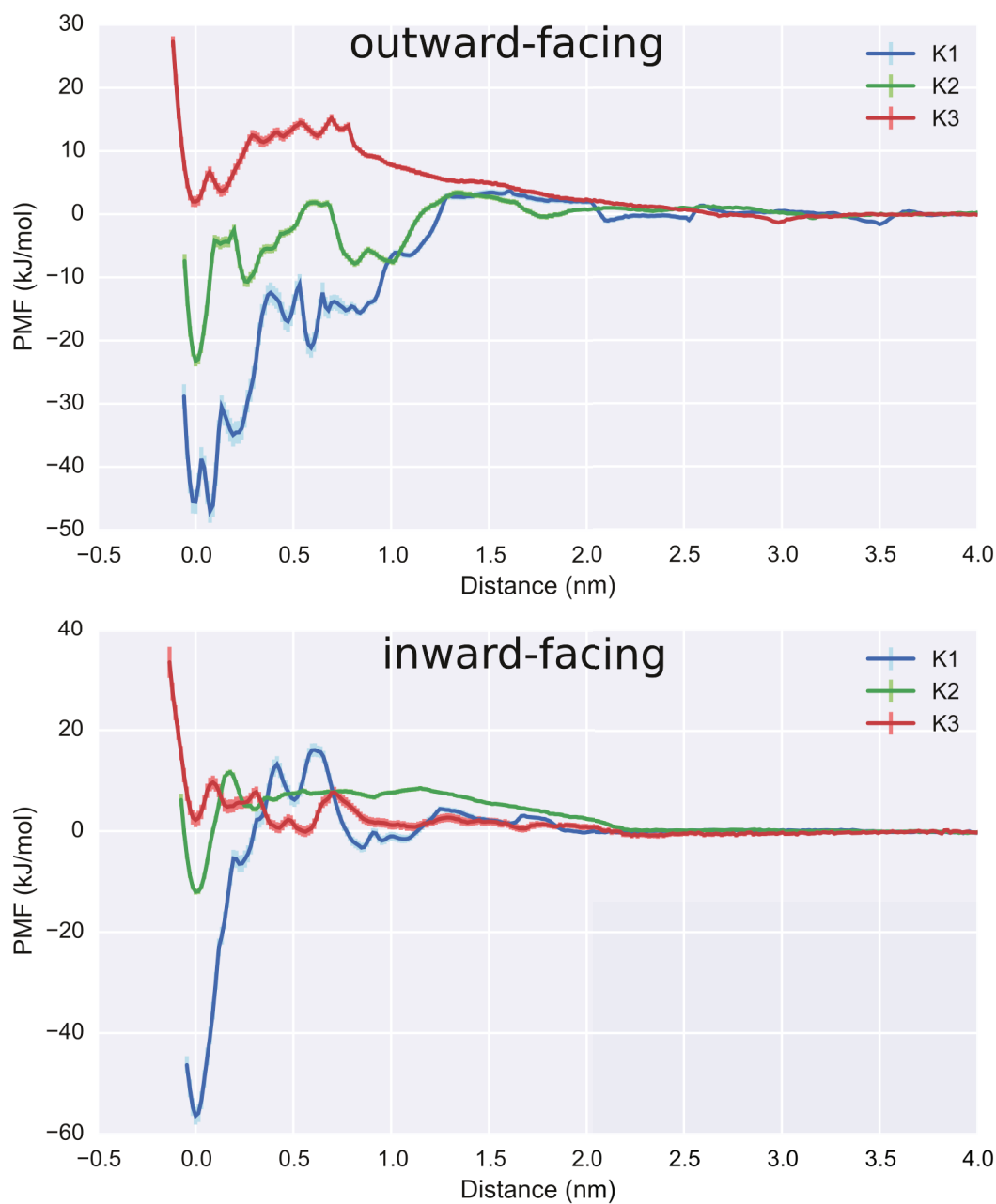


Figure 5.7: Free energy of K^+ binding. *PMF* profiles for K^+ binding in outward- and inward-facing structures for the three binding sites. The profiles are shifted along the *x*-axis such that the first minimum in the *PMF* is at 0nm and along the *y*-axis such that the unbound state corresponds to 0 kJ/mol. Errorbars are plotted as shading.

conformation	K1	K2	K3
outward-facing	$7 \pm 5 \cdot 10^{-8}$	$7 \pm 3 \cdot 10^{-3}$	6 ± 2
inward-facing	$3 \pm 1.8 \cdot 10^{-9}$	0.05 ± 0.01	8 ± 5

Table 5.12: K_D from umbrella sampling (M)

conformation	K1	K2	K3
outward-facing	-45 ± 1.88	-18 ± 0.9	4 ± 0.9
inward-facing	-51 ± 1.6	-7.7 ± 0.6	5 ± 1.5

Table 5.13: ΔG (kJ/mol) from umbrella sampling

Umbrella sampling confirms that K1 has by far the highest affinity for K^+ in inward- as well as outward-facing conformation. Binding to K3 is least favorable and K2 exhibits an intermediate affinity. The PMF of K1 in the outward-facing conformation reflects the two different binding conformations that were found for this site in the free MD simulations. The first minimum in the PMF reflects the conformation, where the D312 side-chain contributes to binding, and the second one represents the conformation, in which N401 is involved in coordinating the ion. The PMF indicates that both conformations are equally stable. Umbrella sampling and the free simulations provide qualitatively the same results, i.e. with K2 exhibiting a higher affinity compared to K3. However, the K_D values for K2 differ between both methods. Such a comparison is not possible for K1, since the estimate from the free MD required an arbitrarily chosen value of the probability to observe no unbinding events.

With this new information we can complete our two pathways of binding model. We assume that K^+ unbinds in the inverse order as binding occurs, i.e. unbinding happens either via K2 or while K3 is occupied. To get the rate of unbinding via K2 consider detailed balance

$$\Delta G_{K1} - \Delta G_{K2} - \Delta G_{K2K1} = 0$$

where ΔG_{K1} , ΔG_{K2} and ΔG_{K2K1} denote the free energy of binding of K1, K2 and the free energy difference between K2 and K1 bound states. Alternatively

we can formulate this in terms of equilibrium constants

$$\frac{K_{K1}}{K_{K2} \cdot K_{K2K1}} = 1$$

plugging in $K_{K2K1} = k_{off}/k_{on}$ and solving for k_{off} gives

$$k_{off} = \frac{k_{on} \cdot K_{K1}}{K_{K2}}$$

With this equation we calculate

$$k_{off} = \frac{3.78 \cdot 10^5 s^{-1} \cdot 1.2 \cdot 10^{-7}}{1.37 \cdot 10^{-1}} = 0.33 s^{-1}$$

For the rate of hopping from K1 to K2 in outward-facing conformation, where known values were taken from Tables 5.12, 5.10, 5.9. Results of unbinding rates for other transitions obtained via this procedure are $1.2 s^{-1}$ for unbinding of K1 when K3 is bound in outward-facing conformation and $0.01 s^{-1}$ for the hopping of an ion from K1 to K2 in inward-facing conformations.

In conclusion we propose that K1 is the binding site which is occupied during the transition from inward- to outward-facing states of the transporter. Since the conformation of the binding site in which D312 participates is the only one observed in inward-facing conformations, we propose that it is this binding conformation in which the transport domain translocates. K2 and K3 are probably only transient binding sites that speed up binding to K1.

5.1.4 Effect of K^+ binding on hairpin opening

The closure of the gate that is formed by the two hairpins is an important determinant for translocation of the transport domain. The Na^+ -glutamate-bound structures all have a closed hairpin. Since an open hairpin conformation leads to steric clashes during the movement of the transport domain, we assume that a closed hairpin is necessary for the isomerization between inward and outward-facing states [31]. While all crystal structures—except the TBOA-bound structure—show a closed conformation of the hairpin tips, they tend to open in MD simulations when no ligands are bound [85, 83]. Binding of Na1 and Na3 is thought to stabilize open conformations. To measure the degree of hairpin opening, we used the distance of the C_α atoms of residues 276 and 355 as reporter for the distance of the hairpin tips (Figure 5.8 A).

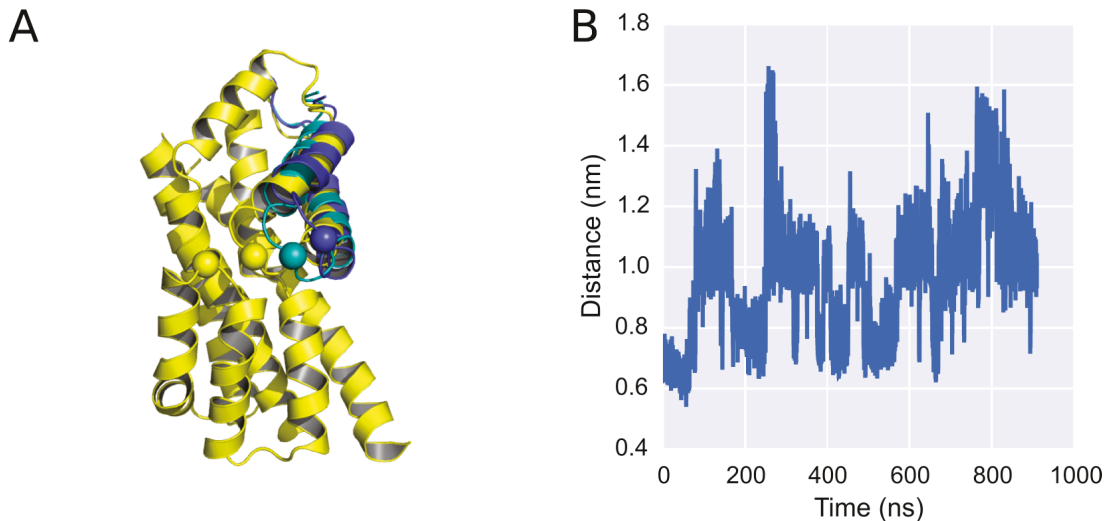


Figure 5.8: Hairpin dynamics. **A**, Representative conformations for the different degrees of opening. The reference atoms for the distance measurement are shown as spheres. The different colors represent distances of 0.8nm (yellow), 1.2nm (cyan) and 1.6nm (blue). **B**, Time course of the distance of the hairpin tips.

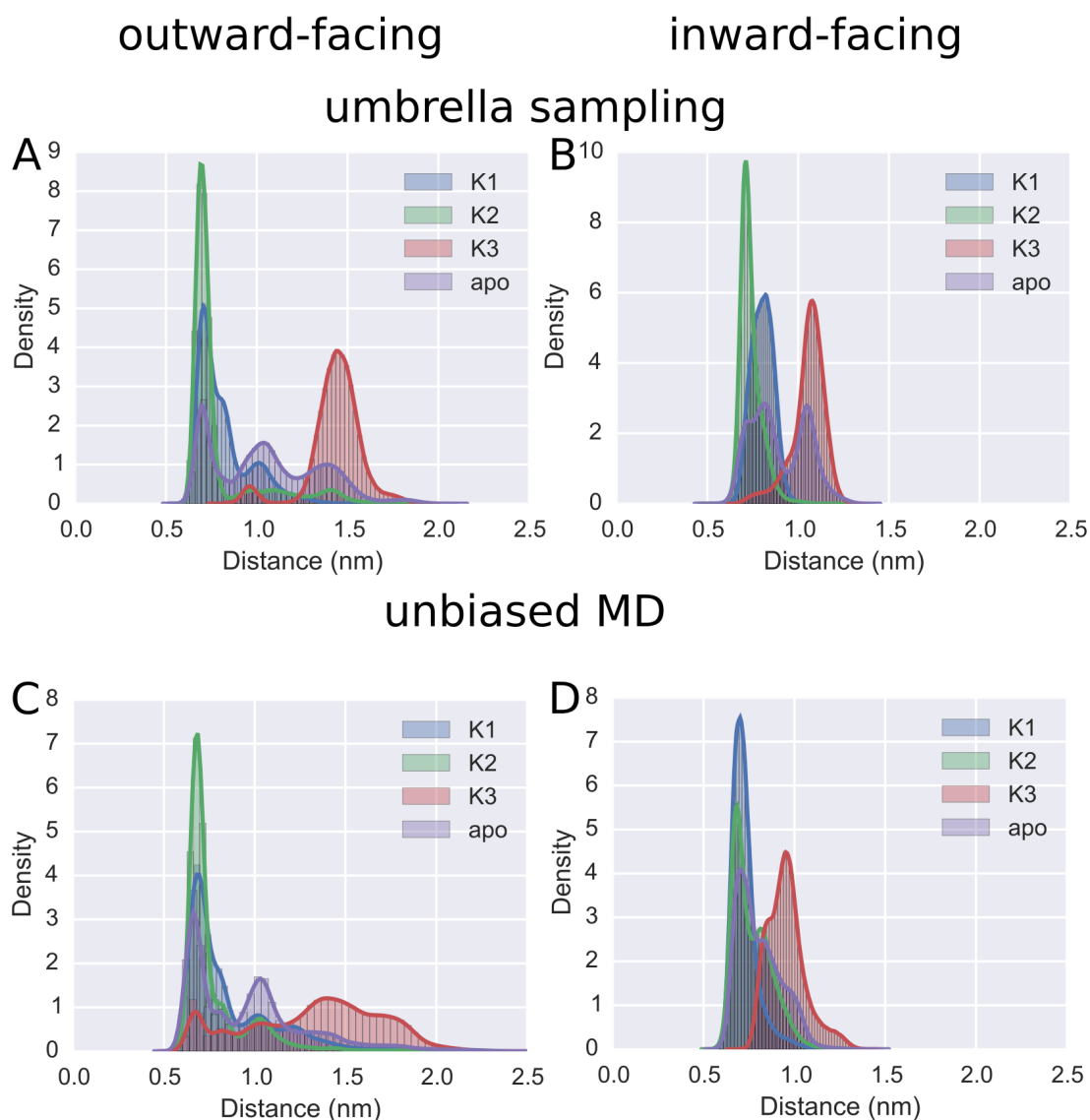


Figure 5.9: K^+ of HP opening. *Histograms for the opening of the hairpin tips for different conformations of the protein. **A and B**, Data from umbrella sampling simulations where an ion is restrained in site resp. bulk. **C and D**, Data from free MD where each trajectory frame is sorted according to the bound conformation. Solid lines represent kernel density estimates.*

Our simulations demonstrate that K^+ binding plays a crucial role in hairpin opening and closing. As long as no ions are bound the hairpins tend to transition between open and closed states and sample a wide range of distances between the hairpin tips (Figure 5.8 B). To quantify the effect of K^+ binding on the

hairpin dynamics, we measured the hairpin distance in the previously described simulations and sorted them according to the bound states (Figure 5.9). If we define the closed state as distance less than 0.9 nm and the open states as distance larger than 0.9 nm, we can calculate the equilibrium constant between both states by counting the number of frames in the open or closed state.

$$K_{eq} = \frac{p_{\text{open}}}{p_{\text{close}}} = \frac{N_{\text{open}}}{N_{\text{close}}}$$

With N_{open} denoting the number of frames, in which the distance was less than the cut-off of 0.9 nm. Tables 5.14 and 5.15 show the resulting equilibrium constants of HP opening calculated from the free MD or umbrella sampling simulations.

conformation	K1	K2	K3	apo
outward-facing	0.47 ± 0.002	0.202 ± 0.0004	4.9 ± 0.3	1.07 ± 0.003
inward-facing	0.035 ± 0.0002	0.136 ± 0.004	2.24 ± 0.02	0.288 ± 0.001

Table 5.14: Equilibrium constants of HP opening from free MD for different bound states

conformation	K1	K2	K3	apo
outward-facing	0.293 ± 0.007	0.216 ± 0.001	244 ± 11	1.99 ± 0.002
inward-facing	0.0568 ± 0.0004	0.0187 ± 0.0001	13.0 ± 0.1	0.777 ± 0.001

Table 5.15: Equilibrium constants of HP opening from umbrella sampling for different bound states

The results show that the hairpin is quite flexible in the apo state while binding to K2 or to K1 stabilizes the closed conformation. In contrast, binding to K3 opens the hairpin. In the inward-facing structure the equilibrium is shifted to closed states when compared to outward-facing structures even in the apo state. The hairpin opening also seems to control the pathway that is taken for K1 binding in outward-facing conformations. If the hairpin is closed, an ion at K2 can readily hop to K1 because the two sites are close to each other. In contrast, binding to K3 is only possible after partial opening of the gate, and occupation of K3 stabilizes the open conformation opening the alternative pathway to K1.

At the same time the distance of K2 to K1 increases rendering hopping from K2 to K1 less likely because K2 is formed by residues at the tip of HP2.

We conclude that K^+ binding induced HP closure providing a possible explanation how K^+ binding enables translocation in EAATs.

5.1.5 HP opening determines K^+ coupling

Our results suggest that Glt_{Ph} binds K^+ with high affinity raising the question why Glt_{Ph} is independent on K^+ . The effect of K^+ binding on the HP opening may provide an explanation: Glt_{Ph} is K^+ independent because the HP samples closed conformations even in the absence of K^+ . A shifted equilibrium of HP opening could lead to strictly K^+ dependent transport by EAATs.

To test this hypothesis, we set up a simplified model for EAAT and Glt_{Ph} transport that allows transitions between inward- and outward-facing apo states as long as the HP is closed. Substrates can only bind to the open conformation (Figure 5.10 A). We then tested if tuning of the equilibrium constant of HP opening in the model can reproduce K^+ independent as well as K^+ dependent transport. In this model Glt_{Ph} and EAAT have identical rates except those for HP opening, translocation reactions and K^+ affinity. The rates of translocation reactions and K^+ affinity were allowed to differ between both models to account for different rate-limiting steps as well as different transport rates. Parameters were then optimized to reproduce Glt_{Ph} transport rates that are independent on intracellular K^+ as well as strict K^+ dependent transport by EAATs. Sodium and glutamate binding was lumped together into one step and a substrate concentration of 200 mM was used. Figure 5.10 summarizes the results, the fitted equilibrium constant of HP opening is 0.46 for Glt_{Ph} and 46 for EAAT. Values of the rates used in this model are shown in Table 5.16. In case of different rates for the Glt_{Ph} or the EAAT model, EAAT rates are given in parenthesis.

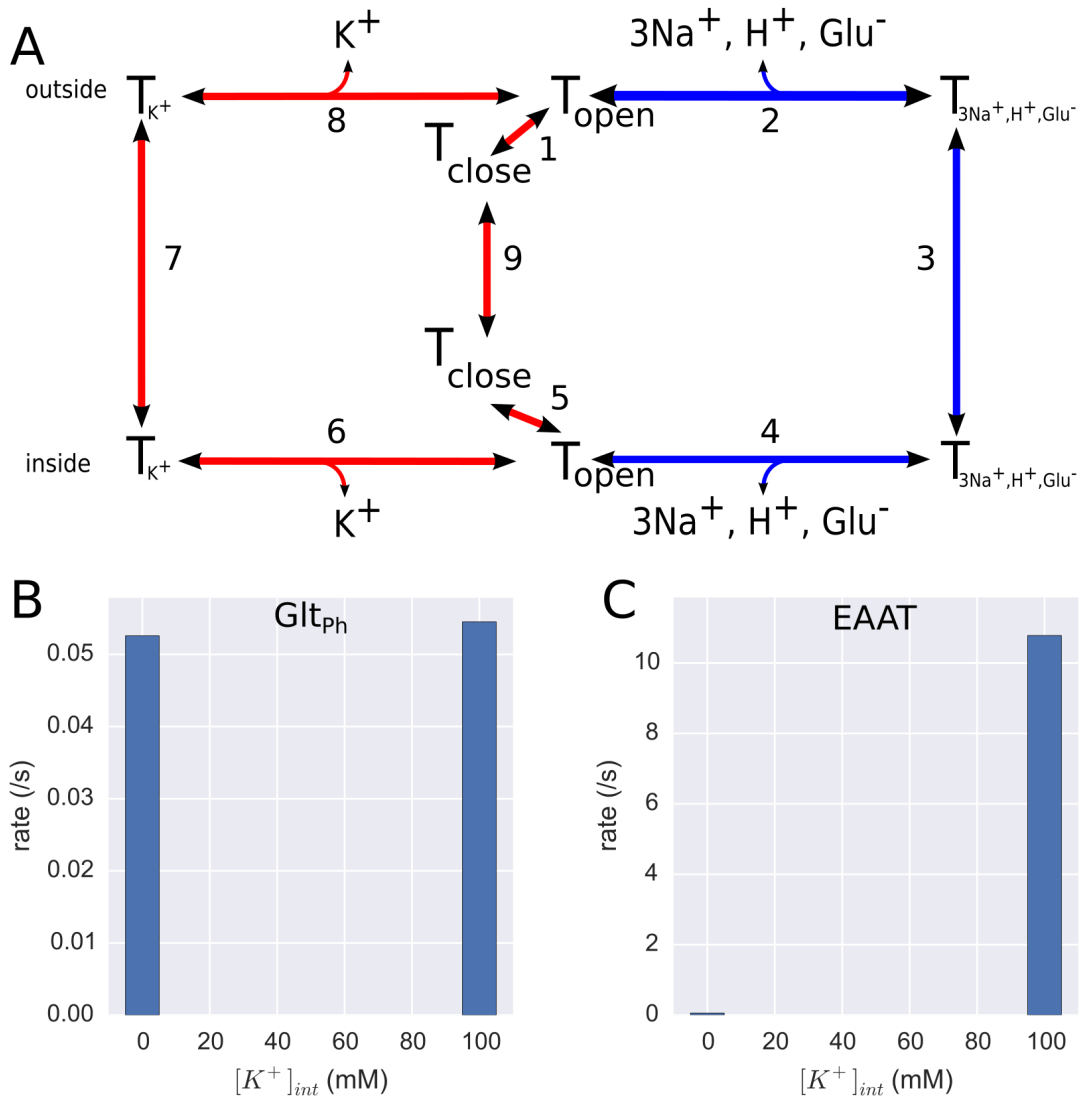


Figure 5.10: HP opening equilibrium in the apo states defines K^+ coupling in EAATs/Glt_{Ph}. **A**, Simplified kinetic model for Glt_{Ph}/EAAT transport. **B**, Simulated Glt_{Ph} transport rates for 0 or 100mM internal K. **C**, Simulated EAAT transport rates for 0 or 100mM internal K.

transition	forward	backward
1	1.42 (145)	3.11
2	$1 \cdot 10^9/\text{M}$	241
3	0.11 (4288)	0.0135 (1054)
4	241	$1 \cdot 10^9/\text{M}$
5	56236	25615 ($2.63 \cdot 10^6$)
6	$1 \cdot 10^9/\text{M}$	1.0 (10000)
7	7.95 (11.6)	4.54 (3.77)
8	0.173 (1728)	$1.73 \cdot 10^8/\text{M}$
9	1.75 (3.06)	14.3 (12.5)

Table 5.16: HP opening equilibrium in the apo states defines K^+ coupling in EAATs/Glt_{Ph}. *Transition rates (s^{-1}) of the model shown in Figure 5.10 (s^{-1}).*

This model accounts for differences between Glt_{Ph} and EAATs and explains how Glt_{Ph} binds K^+ with high affinity but is functionally independent on K^+ .

5.1.6 Effects of *in silico* mutagenesis on free energy of binding

We next introduced three *in silico* mutations in K1: D405N, D312N and N401A. D405N and D312N remove a negative charge from the binding site and should have large impact on K^+ binding. N401A was chosen to further access the role of this residue, from previous simulations it is not clear if this residue is essential for K^+ binding. We set up systems of mutated proteins and subjected them to a initial single long ($1\mu\text{s}$) round of free MD. Figure 5.11 shows a summary of the results. In these simulations both D401N and D312N abolish binding at K1 but do not affect K2 or K3. In N401A all three binding sites get occupied.

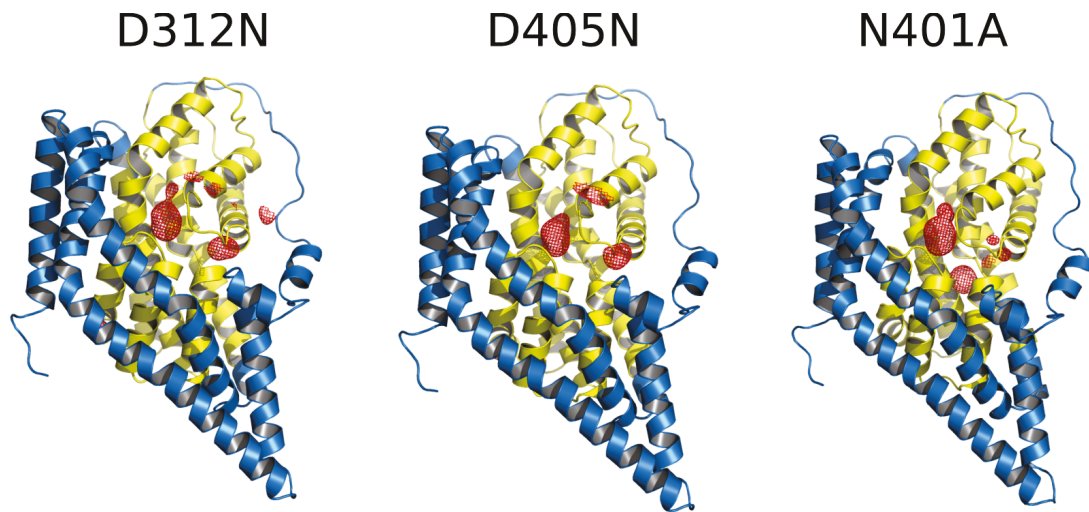


Figure 5.11: Overview on spontaneous K^+ binding to D405N, N401A and D312N. *Results from simulations of spontaneous K^+ binding to mutated proteins. Meshes indicate regions with a high K^+ density inside the transport-domain.*

For a more quantitative evaluation we calculated the change in free energy of K^+ binding induced by the mutations by alchemically transforming an amino-acid side-chain into another. Since we already know the affinity of the wildtype protein from the previous umbrella sampling simulations, only the change in free energy when changing one side-chain into another is necessary for obtaining this value. To calculate the effect of the mutations, we started a series of 160 fast (5-10ns) switching simulations in which the side-chain of interest is mutated following an alchemical path. In each run the work performed on the system is calculated and from the distributions of the forward- and backward-switching the change in free energy is calculated as the intersection point of both distributions [72].

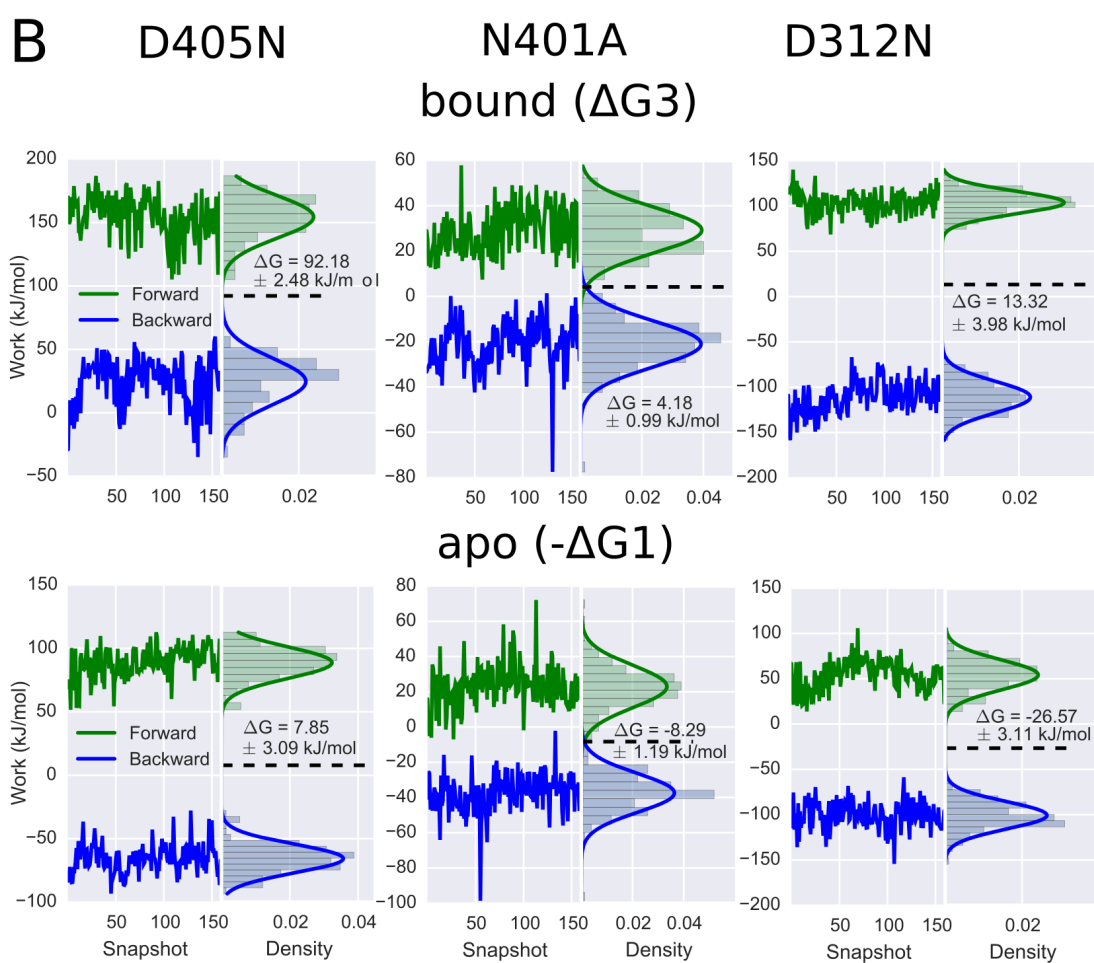
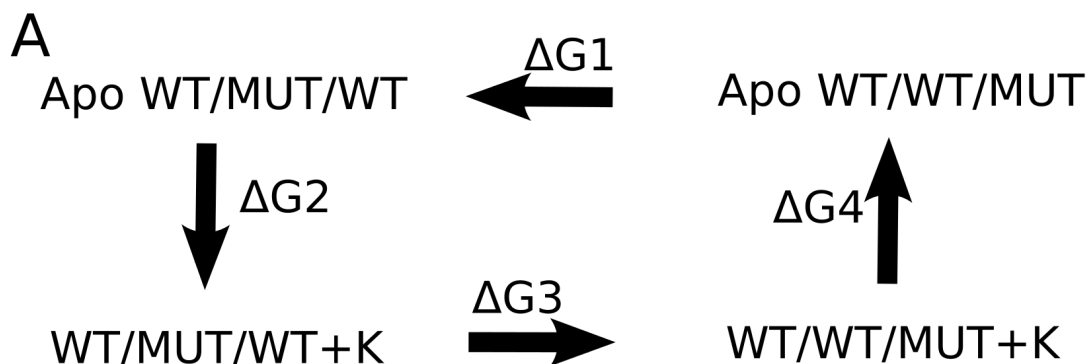


Figure 5.12: Changes in free energy of K^+ binding by D405N, N401A and D312N. **A**, Closed thermodynamic cycle that is used. **B**, Work distributions for the rapid switching between amino acid side-chains for bound and apo state.

Figure 5.12 shows the used thermodynamic cycle and the results for the different mutations. The quantity of interest is the free energy of K^+ binding to a mutated side-chain, i.e. $-\Delta G_4$ in Figure 5.12. The shift in binding free energy for K^+ induced by the mutation is

$$\Delta\Delta G_{bind} = \Delta G_1 + \Delta G_3$$

and the absolute free energy of binding for the mutant proteins is given by

$$-\Delta G_4 = \Delta G_2 + \Delta\Delta G_{bind}$$

where the value for ΔG_2 is taken from umbrella sampling (Table 5.12).

We would expect to get $\Delta G_3 = 0$ if the monomers are functioning independently. Deviations from this value can be explained by different conformations of the two monomers, which were not restrained in this simulations. We already saw that occupation of K1 and HP movement are coupled so the free energy of binding of a K^+ at this site will also depend on the HP conformation. However, by performing the calculations for ΔG_3 we can be sure to get a free energy of binding for the K^+ bound monomer that is not biased by the conformation of the second monomer. Table 5.17 summarizes the results for the changes in free energy.

mutation	ΔG_3	ΔG_1	$\Delta\Delta G_{bind}$	ΔG_{bind}
D405N	92.18 ± 2.48	-7.85 ± 3.09	84.33 ± 3.96	43.3 ± 4.49
N401A	4.18 ± 0.99	8.29 ± 1.19	12.37 ± 1.55	-28.6 ± 2.45
D312N	13.32 ± 3.98	26.57 ± 3.11	40.27 ± 5.05	-0.3 ± 5.59

Table 5.17: Free energy of K^+ binding (kJ/mol) to D405N, N401A and D312N.

The results demonstrate that D405N and D399N abolish K^+ binding almost completely at physiological concentrations, whereas N401A should have only little effect in experiments. N401A has only a small effect on the affinity compared to the other mutations, in agreement with our earlier result that the N401 side-chain is only transiently involved in K^+ binding.

5.1.7 Voltage dependence of K⁺ binding

The previous simulations provided kinetic parameters for a membrane voltage of 0mV. To determine the voltage dependence of each transition and for further comparison with experimental data, we calculated the charge movement associated with transitions in the K⁺ dependent part of the transport cycle.

	outward-facing						inward-facing			
	apo	apo	K3	K2	K1	K1K3	apo	K3	K2	K1
outward-facing	apo	0	-0.092	-0.005	-0.373	-0.487	0.733	-	-	-
	K3	0.092	0	0.087	-0.281	-0.395	-	0.036	-	-
	K2	0.005	-0.087	0	-0.368	-0.483	-	-	-0.236	-
	K1	0.373	0.281	0.368	0	0.114	-	-	-	0.373
	K1K3	0.487	0.395	0.483	-0.114	0	-	-	-	-
inward-facing	apo	-0.733	-	-	-	-	0	0.212	0.027	0.131
	K3	-	-0.036	-	-	-	-0.212	0	-0.185	-0.08
	K2	-	-	0.236	-	-	-0.027	0.185	0	0.104
	K1	-	-	-	-0.373	-	-0.131	0.08	-0.104	0

Table 5.18: Gating charges. *Charge movement (e_0) associated to transitions between states*

Binding to K1 is associated with large charge movement in inward- as well as outward-facing conformations. Although binding to K3 in inward-facing conformations is also associated with substantial charge movement, the low binding rate for this site predicts a negligible contribution to any experimentally measured gating current. For the K2 site we get a negligible amount of charge movement for the binding transition.

The gating charges for translocation steps also provide predictions that can be used to test which site is occupied during the transition of the transport domain. Translocation with a K⁺ bound to K3 is electrically silent whereas K1 and K2 are associated with charge movement of opposite signs.

5.2 Microscale thermophoresis of Glt_{Ph}

We next tested K⁺ binding to Glt_{Ph} experimentally. MST aims at measuring different thermophoretic behaviors of a molecule alone compared to a molecule in complex with a ligand. This is achieved by measuring the fluorescence change in a heated volume at different ligand concentrations (Figure 5.13).

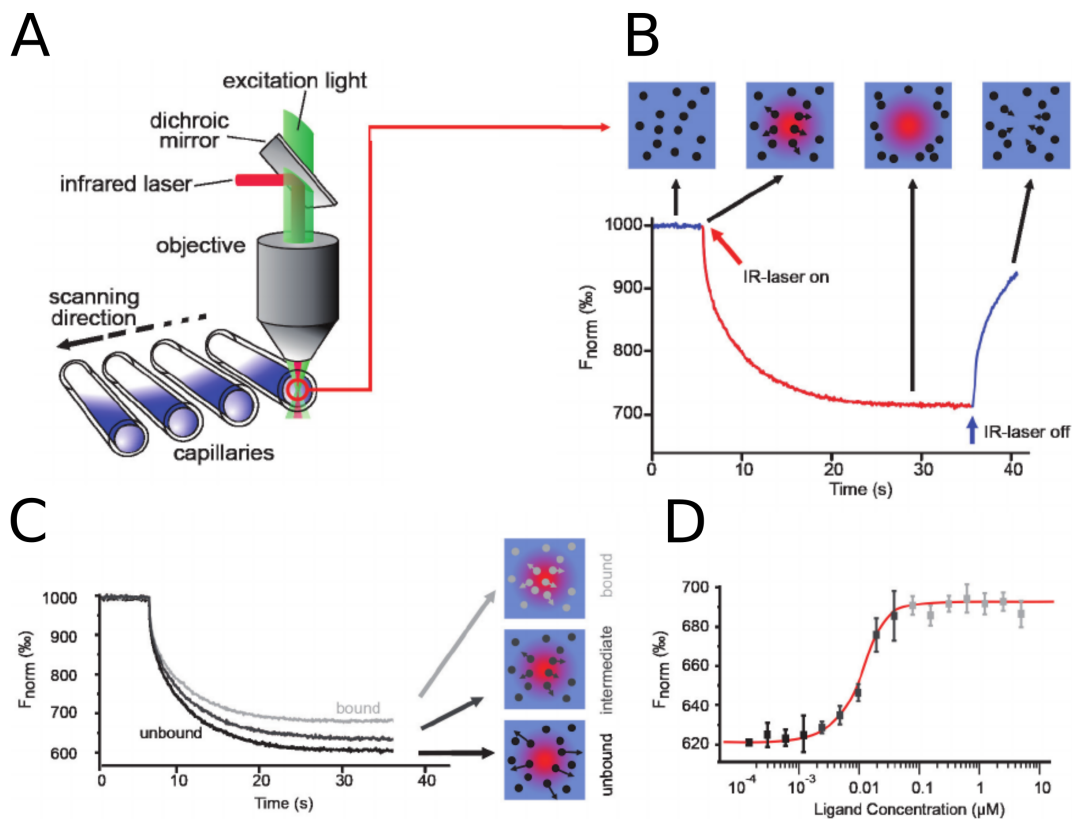


Figure 5.13: MST method. **A**, Capillaries are filled with buffers containing a constant amount of labeled protein and a varying concentration of unlabeled ligands. **B**, A small volume is heated and molecules in this volume diffuse along the temperature gradient which is reflected by changes in the fluorescence signal. **C**, Different thermophoretic properties of bound and unbound protein lead to a different steady state fluorescence after the temperature jump. **D**, Plotting the steady state fluorescence vs. the ligand concentration gives a binding curve. Modified from [78]

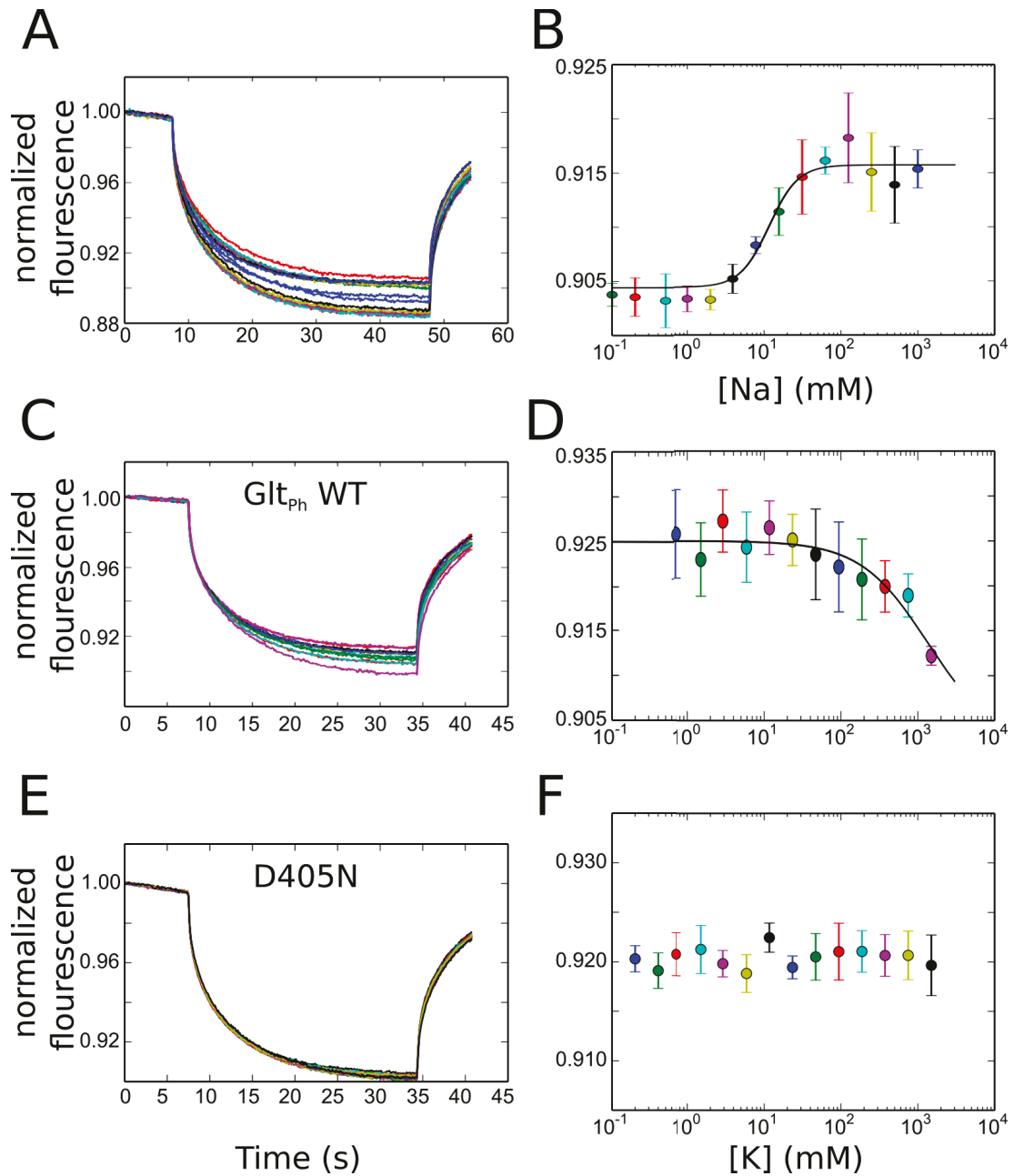


Figure 5.14: MST results. **A,C,D**, Time course of the fluorescence signal after a temperature jump for different ligand concentrations. **B,D,F**, The normalized steady state fluorescence is plotted vs the ion concentration. Solid lines represent fits to hill equations. **A,B**, Na^+ titration to $Gltp_h$ WT. **C,D**, K^+ titration to $Gltp_h$ WT. **E,F**, K^+ titration to $Gltp_h$ D405N. Fit parameters for Na^+ are $K_D = 12mM$, $n = 2.5$.

We first tested if MST can detect Na^+ binding with MST experiments with fluorescence labeled Glt_{Ph} (Figure 5.14 A and B). The resulting fit parameters for Na^+ binding are in line with those that were published by Ewers et al. [86], but are different from those published in [87] or [88]. Consequently, we tested K^+ and could also detect MST signals induced by high K^+ concentrations (Figure 5.14 C and D).

We were not able to reach saturation in the MST signals and therefore cannot get a reliable estimate for the affinity of Glt_{Ph} for K^+ . However, the data show that there is K^+ interaction with Glt_{Ph} . No such effect is seen in Glt_{Ph} D405N further supporting the results of the simulations. In addition the absence of a MST signal with D405N demonstrates that the results of the WT measurements are indeed a specific interaction of K^+ with Glt_{Ph} .

5.3 Experimental validation in EAAT2

We next introduced the homologous mutations D486N, D399N and N482A in EAAT2 and tested the effect on whole-cell patch-clamp recordings of HEK293T cells expressing those constructs. Because channel gating is closely linked to transitions in the transport cycle [11], patch-clamp recordings of EAAT anion currents can be used as a tool to test the effect of a mutation on specific steps in the transport cycle. The transport cycle can be divided into two non-overlapping half-cycles by using appropriate ionic conditions. We are especially interested in comparing anion current recordings under exchange conditions, i.e. symmetric K^+ or symmetric Na^+ and glutamate.

5.3.1 Voltage jumps

In these experiments, we performed voltage jump experiments with voltage steps from 0 to voltages in the range between -170 and +135 mV. The holding potential between sweeps was 0mV and solutions were used that facilitate forward transport or reverse transport or glu-exchange or K^+ -exchange. Figure 5.15 A shows anion current recordings of EAAT2 WT and mutants under those conditions.

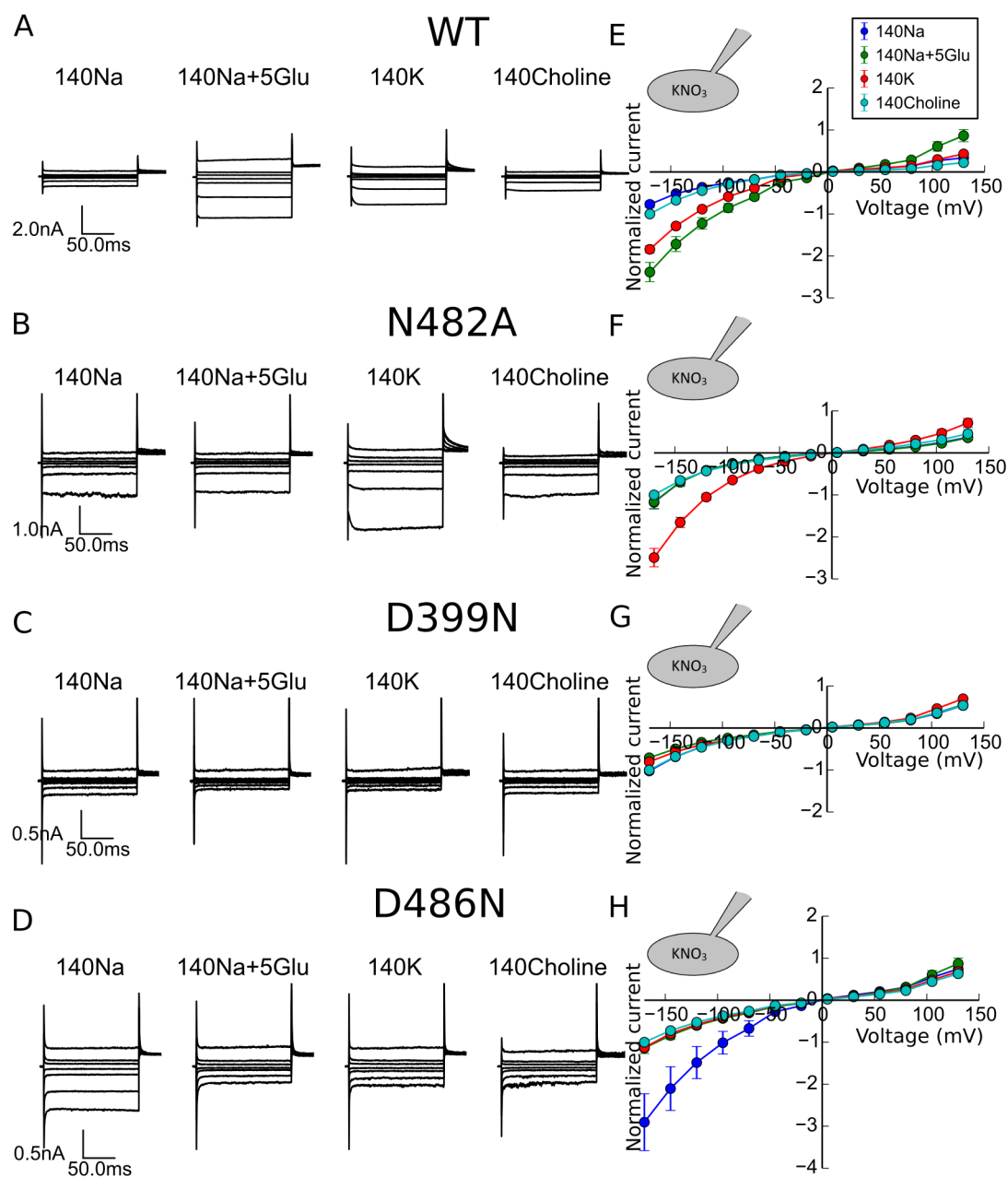


Figure 5.15: Anion current recordings of EAAT2, KNO_3 . **A-D**, Representative anion current recordings of the same cell with a KNO_3 based internal solution, the external solution is indicated in the plots. **E-H**, Voltage dependence of average normalized currents under the different extracellular conditions. Currents are normalized to the current at -170mV in choline nitrate.

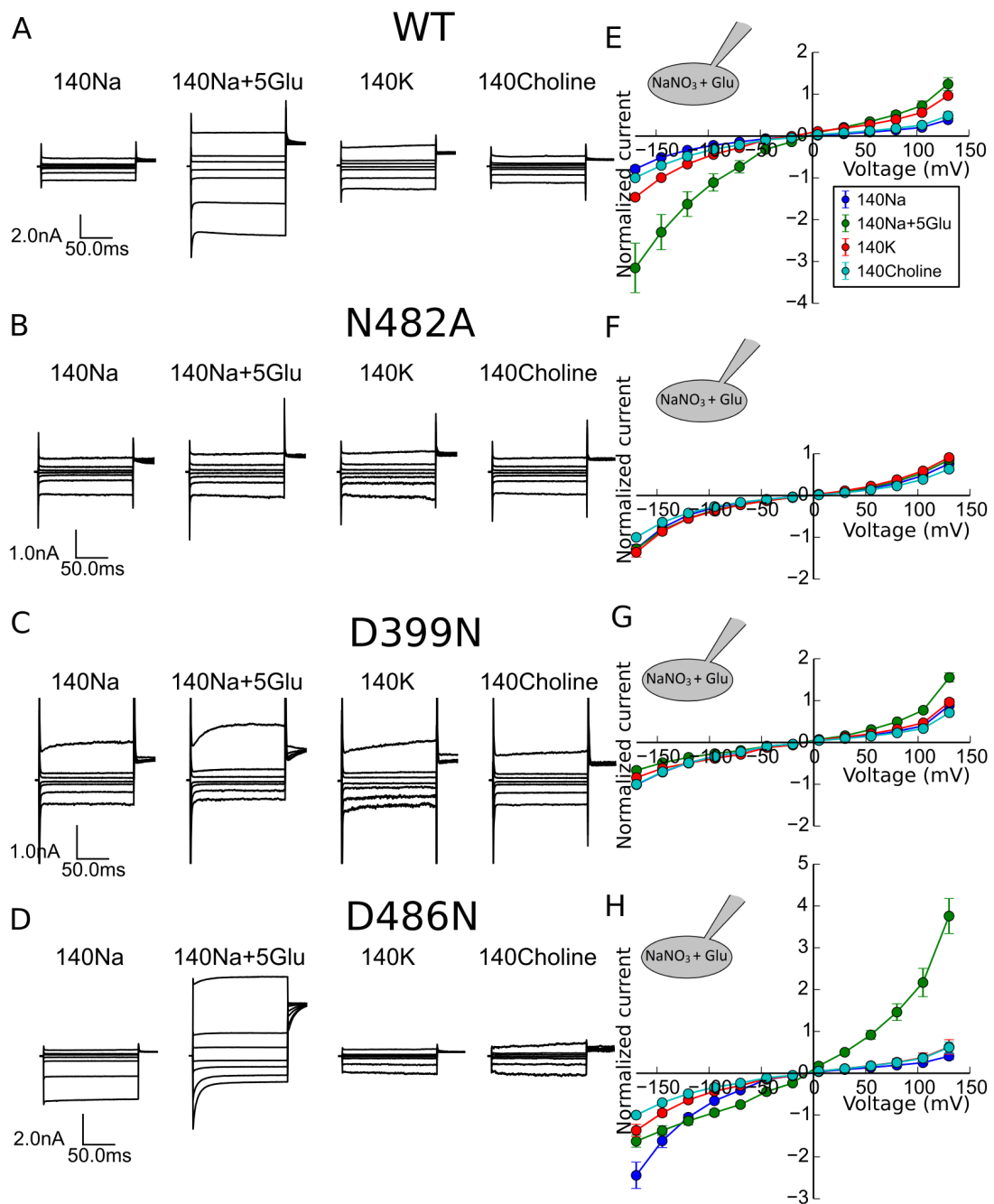


Figure 5.16: Anion current recordings of EAAT2, NaNO₃+glu. **A-D**, Representative anion current recordings of the same cell with a NaNO₃+glu internal based solution the external solution is indicated in the plots. **E-H**, Voltage dependence of average normalized currents under the different extracellular conditions. Currents are normalized to the current at -170mV in choline nitrate.

To have a reference measurement with an inert cation, we used a choline nitrate based solution. In contrast to earlier assumptions, symmetric K^+ activates the anion conductance in EAAT2 WT transporters. This activation of the anion channel can be explained by the conduction pathway found recently in [11], i.e. the channel opens from intermediate conformations where the transport domain is between inward- and outward-facing states. Such intermediate conformations are favored by the use of symmetrical ionic conditions that allow shuttling between inward- and outward-facing conformations. We make use of this fact and take the anion channel activity as a readout for which transitions are affected by mutations in the putative binding sites. Furthermore it can be used to infer the apparent dissociation constant for extracellular K^+ binding. We measured anion current responses at different extracellular K^+ concentrations and plotted the normalized steady state current amplitude versus the K^+ concentration (Figure 5.17).

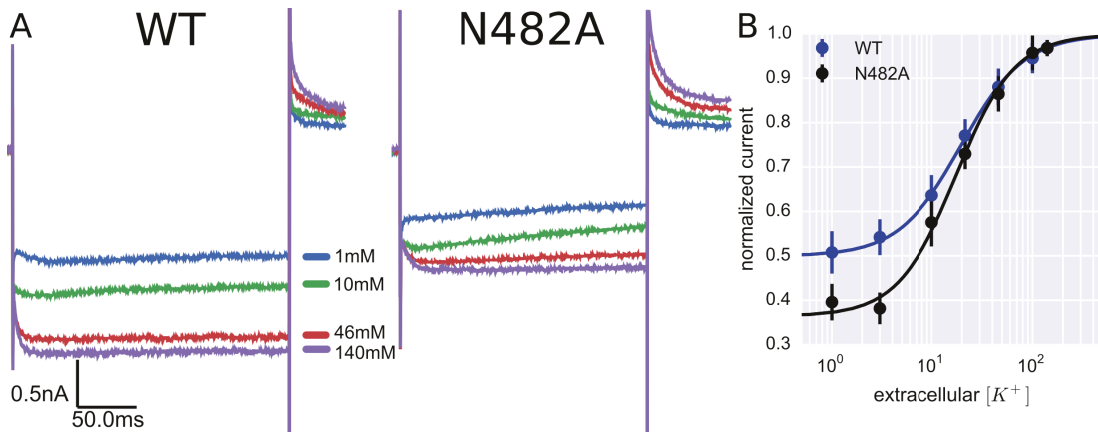


Figure 5.17: K^+ dependence of EAAT2 anion currents. **A**, Representative current recordings at $-170mV$ for different K^+ concentrations. **B**, Normalized steady state currents vs. the K^+ concentration. Solid lines represent fits to the Hill equation. Fit parameters for WT are $K_D = 19.6 \pm 1.9$ and hill coefficient 1.4 ± 0.2 . For N482A we obtain $K_D = 17.4 \pm 2$ and hill coefficient 1.5 ± 0.4 .

In D399N and D486N, the ability of K^+ to activate anion currents is lost (Figure 5.15). The absent anion current activation in D399N with internal KNO_3 is not caused by a non-functional protein as can be seen from the recordings with internal $NaNO_3$. (Figure 5.16) In contrast, symmetric $NaNO_3+glu$ still activates currents in D486N and D399N, albeit with a changed voltage dependency (Fig-

ure 5.16). For both mutations currents activate at positive potentials rather than negative potentials as it is the case in the wild type. Demonstrating that the two mutations still allow transitions between inward- and outward-facing states when $\text{NaNO}_3 + \text{glu}$ are present on both sides of the membrane whereas no such transitions are possible when only K^+ is present on both sides of the membrane. So the mutations had a dramatic effect on K^+ binding or K^+ bound transitions while leaving Na^+ and glutamate binding relatively unaffected.

The N482A construct shows a completely different effect: The interactions with K^+ are almost unchanged but glutamate interactions are lost. The time course of anion currents in the K^+ exchange mode as well as the K^+ dependence of the current are similar to that of EAAT2 WT (Figures 5.15 and 5.17). With Na^+ and glutamate in the pipette none of the tested binding partner is able to elicit a change in the current response (Figure 5.16). This is what would be expected from this mutation because the D486 side-chain is also supposed to ligate glutamate [32].

Anion current recordings confirm the predictions of MD simulations. Mutating the side-chains of D399 or D486 abolishes K^+ induced anion currents, while N482 had no effect on activation by K^+ .

5.3.2 Concentration jumps

Subsequently we measured current responses to fast application of K^+ to EAAT2 expressing HEK293T cells. We used a perfusion pipette pulled from a Θ -glass mounted to a piezo device. The patch-pipette is kept at a constant position in front of the perfusion pipette, and fast solution exchange is achieved by rapidly moving the perfusion pipette. In contrast to voltage jumps this method allows to directly access ligand binding kinetics as long as there is charge movement associated to the binding steps. However, the time resolution is inferior compared to voltage steps. In these experiments, we substituted NO_3 by gluconate which does not permeate EAAT anion channels [89]. The results are summarized in Figure 5.18.

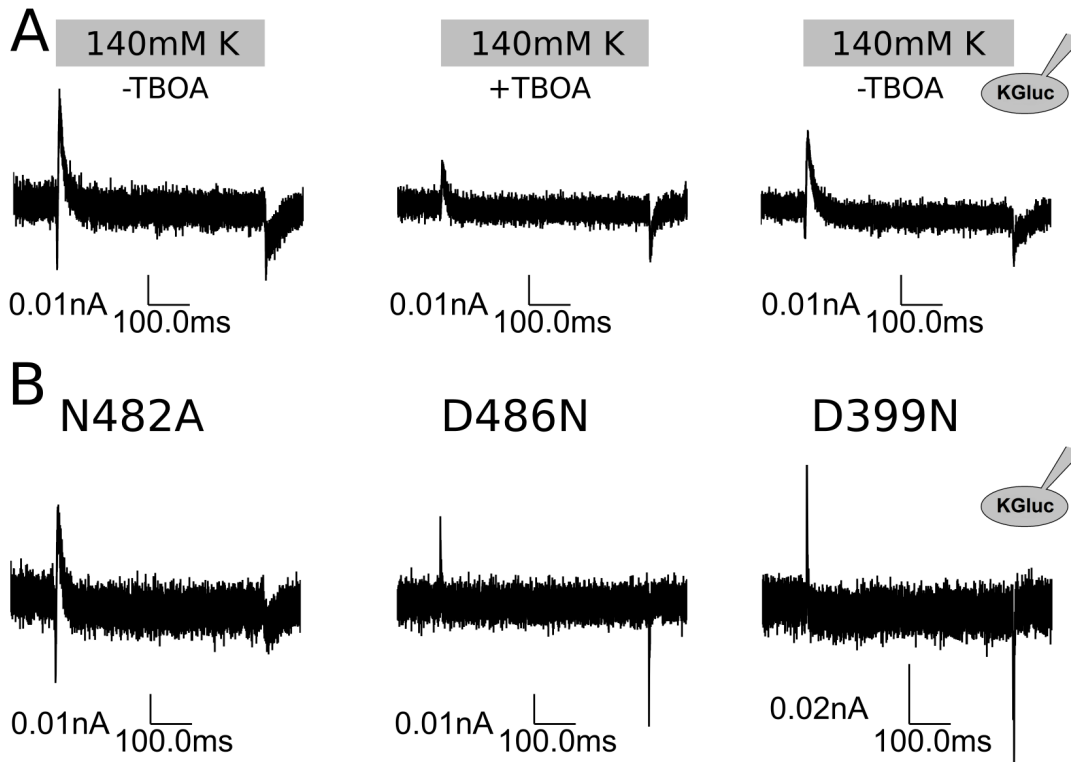


Figure 5.18: Current responses to fast K^+ application. *Application of external K^+ to cells dialyzed with a K^+ based solution. A, Gating currents of EAAT2 WT before and after addition of 5mM Na^+ and 0.1mM of the EAAT blocker TBOA [90]. B, Gating current recordings of EAAT2 mutants.*

When rapidly applying K^+ to EAAT2WT transporters in the absence of permeable anions, we found two spikes of opposite signs. A fast spike at the beginning of a concentration jump indicates movement of positive charges into the cell, suggesting that at least one of the K^+ binding reactions is electrogenic. It could be an artifact from the fast switching between different solutions, but for the following reasons we think that this spike indeed represents binding of a K^+ ion to the transporters: It is reversibly blockable by TBOA (Figure 5.18, A), it is not seen in untransfected cells (data not shown) and not seen in the mutants D482N, D399N (Figure 5.18, B), and the results of the gating charge calculations predict negative charge movement associated with K^+ binding.

The second spike represents the translocation of the negatively charged transport domain [91]. For the mutants we found that the time course of N482A is

similar to the WT recording including the negative spike at the beginning of the concentration jump. In D399N and D486N we get only small and fast spikes with positive sign, no negative current is observed. The D to N mutants still interact with K^+ as predicted by MD, but the interactions that are left are associated with positive charge movement. This would be expected if the mutations abolish binding to K1 since binding to K2 and K3 is associated with negligible charge movement.

Fast solution exchange experiments confirm that the D486N and D399N mutants abolish binding at K1 and that occupation of K1 is the determinant for the translocation of the transport domain.

6. Discussion

We here combined molecular simulations and experiments to characterize the structural basis of K^+ coupled transitions in the transport cycle of EAATs. The K^+ coupled re-translocation is a promising target for pharmacological modification of EAAT transport activity.

6.1 MD simulations reveal three potential binding sites

MD simulations identified three K^+ binding sites within the transport domain of Glt_{Ph}, K1, K2 and K3. K1 and K2 partly overlap with known Na^+ sites. Binding to those sites was observed in simulations of both inward- and outward-facing conformations.

In all simulations binding to the K1 site is most stable in agreement with free energies of binding calculated from umbrella sampling simulations. The fact that the very same binding sites are seen in inward- as well as in outward-facing simulations supports the idea that there is no further movement of the bound K^+ during transitions of the transport domain. We also found distinct binding patterns that elucidate the roles of K2 and K3. Binding to either one of these sites is a precondition for binding at K1. K2 directly relays a K^+ to the K1 site, whereas binding to K3 enables another K^+ to bind to K1. The binding pathway via K3 is only observed in the outward-facing conformation and has a low probability. Binding to K3 induces opening of the hairpin and thus locks the transport domain in outward-facing states. We therefore speculate that K3 is involved in K^+ release to the extracellular solution but the absence of unbinding events at K1 prevents us from testing this hypothesis.

There are several simplifications involved in MD simulations; the most obvious one is the use of classical mechanics force fields. Therefore MD simulations lack electronic polarization effects and the ability to simulate chemical reaction processes like covalent bond formation. Since classical MD simulations do not explicitly model the pH, amino acid residues are typically fixed to the most probable protonation state at the beginning of the simulation, thereby ignor-

ing protonation–conformation coupling. The force fields themselves implement simplified interactions and are trained to reproduce certain properties.

For this thesis the discrimination between Na^+ and K^+ is most critical. Given the fact that we find K^+ binding close to known Na^+ sites, MD simulations of K^+ might just reproduce Na^+ binding. However, classical MD force field have been extremely successful in reproducing Na^+/K^+ selectivity in ion channels [92]. Moreover, the combination of MD simulations with experimental tests allows to critically evaluate the results from computer simulations. We used *in silico* mutagenesis to identify two mutations that abolish K^+ binding in simulations and introduced homolog mutations in EAAT2. Patch-clamp experiments showed that the mutations abolished K^+ binding in EAAT2 while leaving Na^+ binding unaffected. Therefore MD simulations can discriminate Na^+ and K^+ sufficiently well. There are also some other MD results [83] suggesting the K1 site. In this publication it was tested what happens when a K^+ ion is placed manually in a particular site of an EAAT3 homology model and the system is simulated onwards. Here we used a different approach and were able to see spontaneous binding of K^+ in MD simulations. With our approach we are not biased by preselected sites that are considered. Nevertheless the conclusion in [83] regarding the K1 site is the same as in our work. The authors also found that K1 is the most important site for K^+ interactions and also the values for free energy of binding at K1 in inward-facing states inferred here are in the same range as those in [83]. Other sites including K3 are also tested and favorable free energy differences for binding are found, but they are discarded because K1 has by far the highest affinity. What is missing in [83] is kinetic information, binding free energies were only probed with alchemical methods. Our approach enables us to access the roles of the other binding sites and demonstrates that they should not be ignored when investigating K^+ binding to EAATs.

In [82] a site in proximity to the K3 site was postulated based on the observation that the side-chain of R397 is flipped downwards in Glt_{Tk} compared to Glt_{Ph} structures. In this conformation of R397 a cation could bind above R397 and replace the R397 side-chain to interact with T317. This is a tempting speculation because the side-chain of the adjacent residue 318 was also suspected to interact with a K^+ ion since mutations in this residue lead to glutamate homoexchanger phenotypes [42, 93]. However, when interpreting mutants that lead to a

glutamate homo-exchanger phenotype, one has to be careful in associating this with K^+ binding reactions. Experimentally it is hard to distinguish impaired K^+ binding from enhanced Na^+ or glutamate or H^+ binding. A glutamate homoexchanger phenotype is also expected when the rates of unbinding of any of those substrates to the intracellular compartment is very low. In [93] EAAC1(EAAT3) E373Q (homologous to 318 in Glt_{Ph} or 405 in EAAT2, resp.) is investigated. The E to Q mutation shows a glutamate homo-exchanger phenotype, but this residue was later described to be a proton acceptor [94]. According to the established models for glutamate transport by EAATs protonation and K^+ binding are mutually exclusive [6], any mutation that enhances protonation should at the same time impair K^+ binding. If we assume that the E to Q mutation mimics a protonated side-chain, this mutation abolishes intracellular deprotonation and thereby induces the observed phenotype. Another possible alternative explanation for mutations that lead to glutamate exchanger phenotypes are that K^+ still binds, but the mutated residue is involved in subsequent conformational changes. In particular every mutation that impairs K^+ -dependent hairpin closure would also lead to such phenotypes.

Based on our simulations we can rule out the possibility that there is a K^+ binding site above R397. We do not see this kind of binding instead the interaction of the side-chains of R397 and T317 is quite stable which fits well with the results in [84]. This demonstrates that we need more structural information on K^+ binding to reliably implicate glutamate homoexchanger phenotypes in K^+ binding. The results from computer simulation presented here allow connecting the effects measured in patch-clamp experiments to impaired K^+ binding, but we cannot rule out that the residues are involved in both K^+ and H^+ binding.

6.2 K^+ binding to K1 is coupled to hairpin closure

Our MD simulations predict that the hairpin samples open and closed states with similar frequencies when no K^+ is bound, whereas K^+ binding to K1 leads to hairpin closure.

The comparison of the results from umbrella sampling and unbiased simulations provides qualitatively, but not quantitatively, identical results (Figure 5.9,

and Tables 5.14 and 5.15). This difference could be due to insufficient sampling. In our analysis of unbiased simulations we used data from several parallel MD runs to get the distribution of the hairpins for different bound state. We do not control the bound state resulting in different numbers of samples in the distinct distributions. Especially for K3 we have a small number of samples compared to the other states and the relative difference between the two methods is largest for this site (Tables 5.4 and 5.8). In contrast, we control the bound state in umbrella sampling simulations and have equal sampling for all states. Another possible explanation may be slow relaxation times of hairpin movement. In the umbrella sampling simulations we started with a hairpin closed K1 bound structure. If the hairpin opening is slow compared to the timescales that are simulated, we would also expect to get different results for the two approaches.

Hairpin packing is assumed to be the main determinant of translocation [31]. Glt_{Ph} can thus translocate without K⁺ because the hairpins routinely sample the closed state in inward-facing as well as outward-facing apo states. Addition of K⁺ shifts the equilibrium of hairpin distances more to close states (Tables 5.14 and 5.15) and thus makes translocation more likely. This observation accounts for K⁺-bound re-translocation in EAATs. In the absence of K⁺ the distribution of hairpin opening might be shifted to open conformations and K⁺ binding might be necessary for hairpin closure in EAATs. Our results suggest that K⁺ binding to Glt_{Ph} facilitates translocation also in Glt_{Ph}. This is not seen in experiments [38, 32], most likely because the Na⁺ bound translocation is the rate-limiting step in Glt_{Ph}[95].

To clarify these issues, we developed a simplified model for glutamate transport. By using appropriate equilibrium constants for the HP opening as well as translocation rates the same kinetic scheme can produce two different kinds of proteins: Glt_{Ph} binds K⁺ with high affinity but is functional independent on K⁺. In contrast, EAATs that strictly depend on intracellular K⁺ even though they have a lower affinity for K⁺.

6.3 Glt_{Ph} interacts with K⁺

Glt_{Ph} has been assumed to be K⁺-independent for many years. We therefore find an experiment demonstrating K⁺ binding to Glt_{Ph} necessary. We used MST

experiments to demonstrate that Glt_{Ph} can bind K⁺. As a positive control we first tested sodium binding and found that sodium binds Glt_{Ph} with an apparent K_D of 12mM. Titration of K⁺ to Glt_{Ph} induced changes in the MST signal that were absent in experiments with Glt_{Ph} D405N. These results corroborate that Glt_{Ph} interacts with K⁺, and also that the D405 residue is involved in the binding process and thus confirming that Glt_{Ph} can serve as model system for K⁺ interactions in EAATs. The absence of K⁺ binding to Glt_{Ph} D405N is not caused by a missfolded protein induced by the mutation because the same construct was already shown to be a functional transporter in other publications [32].

K_D estimates from the MST experiments and the MD results differ largely at first glance. However, the thermophoretic properties of a given molecule are not known. For Glt_{Ph} there are three potential binding sites that are also coupled to further conformational changes in the protein. In this situation we do not know how the different conformations contribute to the MST signals. If only conformations where K1 and one of the other sites are bound preferably diffuse to the cold volume, we would indeed expect to measure a K_D larger than 1M in a MST experiments. In this regard MST is similar to functional assays in the sense that it may report on specific conformations of the protein rather than only binding of a ligand. Different assays may report on different processes and it is to be expected that they will give different results for fitted apparent dissociation constants. This also explain the wide range of Na⁺ dissociation constants that are found in the literature (22–198 mM) [86, 88, 87].

6.4 Anion current recordings to examine K⁺ interactions in EAAT2

We performed whole-cell patch-clamp experiments under symmetric ionic conditions to probe the effect of mutations on K⁺ coupling. We chose EAAT2 as experimental model system because it is responsible for the major part of glutamate uptake in the brain and should represent the most promising target for pharmacological modification. In EAAT2 WT conditions favoring translocation steps lead to an increase in anion current amplitudes. The tested mutations selectively knocked out the activation in one of the half-cycles while leaving the other one intact.

In a mutagenesis experiment we cannot exclude indirect effects on the protein and have to be careful when associating a residue in a specific step of the transport. However, the fact that we only knocked out specific steps in the transport cycle and only mildly affected the other half-cycle shows that the overall protein structure and function was not changed. Furthermore, the combination of experimental data with MD simulations allows to associate the mutated residues with K^+ interactions.

One important result from patch-clamp experiments is that symmetric K^+ activates anion currents in EAAT2 WT. From the results in [11] we would expect that all the isoforms exhibit this behavior, but so far we did not test it. At this point we want to emphasize some facts for EAAT2 that are under-appreciated in the literature (Figures 5.15 and 5.16): EAAT2 mediates an anion conductance even in the complete absence of any substrates. In the absence of transportable substrates, external Na^+ inhibits anion currents, rather than activates, anion currents. Furthermore, K^+ bound conformations contribute significantly to the anion conductance of EAAT2.

The first two observations were already found in [96] and are confirmed here. Originally, Billups et al. proposed the idea that K^+ bound conformations are non-conducting for retinal glutamate transporters in 1996 [97], and this is still assumed in recent publications [98]. Even though already in 2002, Bergles et al. also proposed activation of anion currents by K^+ , when modeling Glt-1 (rat EAAT2) currents by adding a channel state to the inward-facing K^+ bound state of their model, these authors also assumed that Na^+ is required for channel opening [99]. In [96] anion conducting states were added to both inward- and outward-facing K^+ bound states without measuring it directly. Here we present clear and direct evidence that EAAT2 anion channels open from K^+ bound conformations. Based on the current concept that intermediate conformations lead to channel opening and that channel opening is not possible from inward- or outward-facing states [11], we should refrain from adding channel states to outward- or inward-facing states and rather add an additional intermediate state from which the channel can open. If we assume that the anion channel opens only from intermediate conformations, then inhibition of anion currents by Na^+ appears to support efficient transporter: The decrease in anion channel activity induced by Na^+ can be explained by a model where Na^+ traps the transporter in outward-facing confor-

mations that then can readily bind glutamate. The same conclusion is drawn for Glt_{Ph} where the transport domain seems to be less flexible when Na⁺ is bound compared to the apo protein and addition of aspartate restores the flexibility [100, 95].

The activation of anion currents by K⁺ allows to probe the K⁺ hemi-cycle in isolation by measuring anion currents in appropriate ionic conditions. It provides another assay to measure the extracellular K⁺ affinity besides reverse transport and to distinguish how different half-cycles of the transport cycle are affected by mutations in the protein. So far, the distinction of a glutamate homo-exchange from forward transporter was based on comparing radioactive uptake experiments in cells with internal glutamate to experiments in liposomes without internal glutamate [42, 101]. At least for EAAT2 this costly approach can be replaced with patch-clamp recordings of anion currents in the glu- resp. K⁺-exchange mode.

6.5 Mutations in side-chains contributing to the K1 site affect one half-cycle, but leave the other intact

We performed the same kind of anion current measurements with three different mutations introduced in EAAT2 and found that D486N and D399N are glutamate exchangers, while N482A is a K⁺ exchanger. These experimental observations coincide with the theoretical predictions made by MD simulations. MD simulations of the N401A mutation predict no effect on K⁺ coupling while D405N and D312N abolish binding at the K1 site. These results show that this K⁺ site is conserved between EAATs and Glt_{Ph}. They also support the idea that the K1 site is the most important binding site in the sense that this site is occupied during the transition between inward- and outward-facing conformations of the transport domain. N482A had no effect on the apparent K_D while the *in silico* results of N401A predicted at least a small shift in the affinity for K1. However, the value from MD represent the dissociation constant of the binding reaction, whereas the fitted value from experiment used the anion conductance as readout, in which several more transitions are involved (HP closure, transition of transport

domain, channel opening). We do not necessarily expect a change in K_D of anion channel activation even though the K_D of binding might have changed. The measured WT K_D is several orders of magnitude larger than that calculated in MD simulations which is a general problem when comparing parameters inferred from simulations of a isolated transitions with experimental values that in most cases represent an equilibrium of several states [35].

6.6 K^+ binding and K^+ bound translocation in EAAT2 are electrogenic

When rapidly applying K^+ to cells expressing EAAT2 WT, we found that there at least two electrogenic processes that are associated with charge movement of opposite signs. The D486N and D399N mutation abolished the first process whereas N482A had little effect on observed currents. The second process that is associated with the movement of negative charge was already described earlier and interpreted to represent the transition of the transport domain [91, 99].

One tempting interpretation for the first process is that it represents K^+ binding to the protein. Alternatively it could represent conformational changes that happen before K^+ binding. The apo transport domain is negatively charged and if we assume that it can translocate partially to explain channel opening in the apo state, closure of the channel before K^+ binding would give a gating charge of the same sign as a electrogenic K^+ binding process. However, the small open probability of EAAT anion channels [102] renders it unlikely that channel closure contributes substantially to the measured charge movement. Furthermore, the calculated gating charges from MD simulations indicate that K^+ binding to K1 as well as K1 bound translocation are associated with the observed charge movement. The values of the gating charges combined with the high affinity of K1 suggest that the observed first spike in the current is mainly associated with K1 binding. In addition, the calculated gating charges for translocation steps indicate that the second spike in the current is associated with a K1 bound transition from outward- to inward-facing. This interpretation is further corroborated by the absence of this kind of charge movement in the recordings of D486N and D399N.

The D to N mutants still show a response to K^+ application with an amplitude

that is too large to be accounted as an artifact from the solution exchange. The anion current recordings imply that this positive current is not associated with movement of the transport domain because K^+ did not activate anion currents. An alternative explanation is that the observed charge movement is associated with HP opening after K3 binding. MD simulations of the mutants showed that binding at K3 is not impaired by the mutation and binding to K3 induces HP opening, which is also associated with a small amount of charge movement [103].

Our results for WT EAAT2 contradict the conclusion from [91] where it is inferred that binding of K^+ is not electrogenic and only the translocation reaction is. Grewer et al. used the following reasoning: EAAC1 E373Q does bind K^+ because K^+ inhibits glu induced currents [93] whereas in the mutant no charge movement is seen when applying voltage steps in the K^+ -exchange mode. Moreover, in the same conditions in the WT charge movement is measured. Hence in the WT the binding reaction itself is not electrogenic. This conclusion is valid if one assumes that there is only one K^+ binding site in EAATs. The results presented here provide an alternative explanation: If the E373Q mutation impairs binding at K1, which is shown in [94], and leaves binding at the other sites intact this accounts for the inhibition of glu induced currents. K^+ binding at K3 and glu binding are mutually exclusive because the binding sites overlap in that region [31]. If only binding to K1 is associated with substantial charge movement in the wildtype, as shown by the results from MD simulations and by the current responses to fast K^+ application of the D486N and D399N mutants, this accounts for the other observations. A model with three binding sites where only binding to one of the sites is electrogenic explains both our results and those found in [91]. There are several possible other reasons for the discrepancy between our results and those from [91]. First, they measured a different EAAT isoform and we cannot rule out the possibility that we are dealing here with an EAAT2 specific behavior. However, all binding site forming residues presented here are completely conserved in all EAAT isoforms. We therefore do not expect that the qualitative conclusions drawn here differ between isoforms. Second, their solution exchange time of 50ms may be too slow to resolve the fast first spike. Finally, the currents shown in [91] also exhibit a fast negative spike at the beginning of the concentration jump which is sensitive to TBOA. This spike is small in amplitude and might have been interpreted as an artifact.

7. Conclusion

We here used MD simulations of Glt_{Ph} to describe the mechanism of K⁺ dependent re-translocation in EAATs. We identified three distinct binding sites, described the binding order of these sites and showed that the K1 site is conserved across the EAAT family. The combination of calculated affinities for the different binding sites with calculated gating charges and the patch-clamp recordings of EAAT2 demonstrates that the K1 site is occupied during the K⁺ bound translocation of the transport domain. The three binding site model explains the behavior of different mutations in EAAT2 as well as some seemingly contradictory results found here and in the literature.

Glt_{Ph} proved to be a good model for the K⁺ binding reaction in EAATs and also interacts with K⁺ itself. We showed that tuning of the parameters of gate closure and K⁺ binding can lead to K⁺ binding but not K⁺ dependent transporters or to strictly K⁺ dependent transport. This observation sheds light onto further steps of the EAAT transport cycle, K⁺ binding leads to hairpin closure which in turn makes the transport domain translocation competent.

Bibliography

- [1] Niels C Danbolt. “Glutamate uptake”. In: *Progress in Neurobiology* 65.1 (Sept. 2001), pp. 1–105.
- [2] Maria Ankarcrona et al. “Glutamate-induced neuronal death: A succession of necrosis or apoptosis depending on mitochondrial function”. In: *Neuron* 15.4 (Oct. 1995), pp. 961–973.
- [3] Marc Laruelle, Lawrence S. Kegeles, and Anissa Abi-Dargham. “Glutamate, Dopamine, and Schizophrenia”. In: *Annals of the New York Academy of Sciences* 1003.1 (Nov. 2003), pp. 138–158.
- [4] Heather L. Scott et al. “Aberrant Expression of the Glutamate Transporter Excitatory Amino Acid Transporter 1 (EAAT1) in Alzheimer’s Disease”. In: *Journal of Neuroscience* 22.3 (2002), RC206–RC206.
- [5] Anthony J. Groom, Terence Smith, and Lechoslaw Turski. “Multiple Sclerosis and Glutamate”. In: *Annals of the New York Academy of Sciences* 993.1 (May 2003), pp. 229–275.
- [6] Baruch I. Kanner and Annie Bendahan. “Binding order of substrates to the (sodium + potassium ion)-coupled L-glutamic acid transporter from rat brain”. In: *Biochemistry* 21.24 (Nov. 1982), pp. 6327–6330.
- [7] Noa Zerangue and Michael P. Kavanaugh. “Flux coupling in a neuronal glutamate transporter”. In: *Nature* 383.6601 (Oct. 1996), pp. 634–637.
- [8] Line M. Levy, Orpheus Warr, and David Attwell. “Stoichiometry of the Glial Glutamate Transporter GLT-1 Expressed Inducibly in a Chinese Hamster Ovary Cell Line Selected for Low Endogenous Na⁺-Dependent Glutamate Uptake”. In: *Journal of Neuroscience* 18.23 (1998), pp. 9620–9628.
- [9] W. A. Fairman et al. “An excitatory amino-acid transporter with properties of a ligand-gated chloride channel”. In: *Nature* 375.6532 (June 1995), pp. 599–603.

- [10] Jan-Philipp Machtens, Peter Kovermann, and Christoph Fahlke. “Substrate-dependent Gating of Anion Channels Associated with Excitatory Amino Acid Transporter 4”. In: *Journal of Biological Chemistry* 286.27 (May 2011), pp. 23780–23788.
- [11] Jan-Philipp Machtens et al. “Mechanisms of anion conduction by coupled glutamate transporters.” eng. In: *Cell* 160.3 (Jan. 2015), pp. 542–553.
- [12] Margaret Lin Veruki, Svein Harald Mørkve, and Espen Hartveit. “Activation of a presynaptic glutamate transporter regulates synaptic transmission through electrical signaling”. In: *Nature Neuroscience* 9.11 (Oct. 2006), pp. 1388–1396.
- [13] Verena Untiet et al. “Glutamate transporter-associated anion channels adjust intracellular chloride concentrations during glial maturation”. In: *Glia* 65.2 (Nov. 2016), pp. 388–400.
- [14] Knut P. Lehre and Niels C. Danbolt. “The Number of Glutamate Transporter Subtype Molecules at Glutamatergic Synapses: Chemical and Stereological Quantification in Young Adult Rat Brain”. In: *Journal of Neuroscience* 18.21 (1998), pp. 8751–8757.
- [15] Carsten Mim et al. “The Glutamate Transporter Subtypes EAAT4 and EAATs 1-3 Transport Glutamate with Dramatically Different Kinetics and Voltage Dependence but Share a Common Uptake Mechanism”. In: *The Journal of General Physiology* 126.6 (Nov. 2005), pp. 571–589.
- [16] Yvette Dehnes et al. “The Glutamate Transporter EAAT4 in Rat Cerebellar Purkinje Cells: A Glutamate-Gated Chloride Channel Concentrated near the Synapse in Parts of the Dendritic Membrane Facing Astroglia”. In: *Journal of Neuroscience* 18.10 (1998), pp. 3606–3619.
- [17] A. Lee et al. “Excitatory Amino Acid Transporter 5 is widely expressed in peripheral tissues”. In: *European Journal of Histochemistry* 57.1 (Mar. 2013), p. 11.
- [18] Jae-Hyuk Yi and Alan S. Hazell. “Excitotoxic mechanisms and the role of astrocytic glutamate transporters in traumatic brain injury”. In: *Neurochemistry International* 48.5 (Apr. 2006), pp. 394–403.

- [19] K. Tanaka. “Epilepsy and Exacerbation of Brain Injury in Mice Lacking the Glutamate Transporter GLT-1”. In: *Science* 276.5319 (June 1997), pp. 1699–1702.
- [20] Hong Yu et al. “GLAST Deficiency in Mice Exacerbates Gap Detection Deficits in a Model of Salicylate-Induced Tinnitus”. In: *Frontiers in Behavioral Neuroscience* 10 (Aug. 2016).
- [21] Pietro Peghini, Julia Janzen, and Wilhelm Stoffel. “Glutamate transporter EAAC-1-deficient mice develop dicarboxylic aminoaciduria and behavioral abnormalities but no neurodegeneration”. In: *The EMBO Journal* 16.13 (July 1997), pp. 3822–3832.
- [22] Y. H. Huang. “Climbing Fiber Activation of EAAT4 Transporters and Kainate Receptors in Cerebellar Purkinje Cells”. In: *Journal of Neuroscience* 24.1 (Jan. 2004), pp. 103–111.
- [23] J.C. Jen et al. “Primary episodic ataxias: diagnosis, pathogenesis and treatment”. In: *Brain* 130.10 (Oct. 2007), pp. 2484–2493.
- [24] N. Winter, P. Kovermann, and C. Fahlke. “A point mutation associated with episodic ataxia 6 increases glutamate transporter anion currents”. In: *Brain* 135.11 (Oct. 2012), pp. 3416–3425.
- [25] Abby Adamczyk et al. “Genetic and functional studies of a missense variant in a glutamate transporter, SLC1A3, in Tourette syndrome”. In: *Psychiatric Genetics* 21.2 (Apr. 2011), pp. 90–97.
- [26] Dinesh Yernool et al. “Structure of a glutamate transporter homologue from *Pyrococcus horikoshii*”. In: *Nature* 431.7010 (Oct. 2004), pp. 811–818.
- [27] Christof Grewer et al. “Individual Subunits of the Glutamate Transporter EAAC1 Homotrimer Function Independently of Each Other†”. In: *Biochemistry* 44.35 (Sept. 2005), pp. 11913–11923.
- [28] Guus B. Erkens et al. “Unsynchronised subunit motion in single trimeric sodium-coupled aspartate transporters.” eng. In: *Nature* 502.7469 (Oct. 2013), pp. 119–123.

- [29] Yi Ruan et al. “Direct visualization of glutamate transporter elevator mechanism by high-speed AFM”. In: *Proceedings of the National Academy of Sciences* 114.7 (Jan. 2017), pp. 1584–1588.
- [30] Nicolas Reyes, Christopher Ginter, and Olga Boudker. “Transport mechanism of a bacterial homologue of glutamate transporters”. In: *Nature* 462.7275 (Nov. 2009), pp. 880–885.
- [31] Grégory Verdon et al. “Coupled ion binding and structural transitions along the transport cycle of glutamate transporters.” eng. In: *Elife* 3 (May 2014), e02283.
- [32] Olga Boudker et al. “Coupling substrate and ion binding to extracellular gate of a sodium-dependent aspartate transporter”. In: *Nature* 445.7126 (Jan. 2007), pp. 387–393.
- [33] Zhijian Huang and Emad Tajkhorshid. “Identification of the Third Na^+ Site and the Sequence of Extracellular Binding Events in the Glutamate Transporter”. In: *Biophysical Journal* 99.5 (Sept. 2010), pp. 1416–1425.
- [34] H. P. Larsson et al. “Evidence for a third sodium-binding site in glutamate transporters suggests an ion/substrate coupling model”. In: *Proceedings of the National Academy of Sciences* 107.31 (July 2010), pp. 13912–13917.
- [35] Turgut Bastug et al. “Position of the Third Na^+ Site in the Aspartate Transporter Glt_{Ph} and the Human Glutamate Transporter, EAAT1”. In: *PLoS ONE* 7.3 (Mar. 2012). Ed. by Hendrik W. Editor van Veen, e33058.
- [36] Albert Guskov et al. “Coupled binding mechanism of three sodium ions and aspartate in the glutamate transporter homologue Glt_{Tk}”. In: *Nature Communications* 7 (Nov. 2016), p. 13420.
- [37] Maarten Groeneveld and Dirk-Jan Slotboom. “ Na^+ :Aspartate Coupling Stoichiometry in the Glutamate Transporter Homologue GltPh”. In: *Biochemistry* 49.17 (May 2010), pp. 3511–3513.
- [38] R. M. Ryan, E. L. R. Compton, and J. A. Mindell. “Functional Characterization of a Na^+ -dependent Aspartate Transporter from *Pyrococcus horikoshii*”. In: *Journal of Biological Chemistry* 284.26 (Apr. 2009), pp. 17540–17548.

- [39] Zhen Tao, Armanda Gameiro, and Christof Grewer. “Thallium ions can replace both sodium and potassium ions in the glutamate transporter excitatory amino acid carrier 1.” eng. In: *Biochemistry* 47.48 (Dec. 2008), pp. 12923–12930.
- [40] H. Burr Steinbach and Sol Spiegelman. “The sodium and potassium balance in squid nerve axoplasm”. In: *Journal of Cellular and Comparative Physiology* 22.2 (Oct. 1943), pp. 187–196.
- [41] C. Grewer et al. “Glutamate translocation of the neuronal glutamate transporter EAAC1 occurs within milliseconds”. In: *Proceedings of the National Academy of Sciences* 97.17 (Aug. 2000), pp. 9706–9711.
- [42] M. P. Kavanaugh et al. “Mutation of an Amino Acid Residue Influencing Potassium Coupling in the Glutamate Transporter GLT-1 Induces Obligate Exchange”. In: *Journal of Biological Chemistry* 272.3 (Jan. 1997), pp. 1703–1708.
- [43] Yumin Zhang et al. “Molecular determinant of ion selectivity of a (Na^+ + K^+)-coupled rat brain glutamate transporter”. In: *Proceedings of the National Academy of Sciences* 95.2 (1998), pp. 751–755.
- [44] R. Zarbiv et al. “Cysteine Scanning of the Surroundings of an Alkali-Ion Binding Site of the Glutamate Transporter GLT-1 Reveals a Conformationally Sensitive Residue”. In: *Journal of Biological Chemistry* 273.23 (June 1998), pp. 14231–14237.
- [45] A. Bendahan. “Arginine 447 Plays a Pivotal Role in Substrate Interactions in a Neuronal Glutamate Transporter”. In: *Journal of Biological Chemistry* 275.48 (Sept. 2000), pp. 37436–37442.
- [46] Shlomit Teichman, Shaogang Qu, and Baruch I. Kanner. “The equivalent of a thallium binding residue from an archeal homolog controls cation interactions in brain glutamate transporters.” eng. In: *Proc Natl Acad Sci U S A* 106.34 (Aug. 2009), pp. 14297–14302.
- [47] Noa Rosental, Annie Bendahan, and Baruch I. Kanner. “Multiple consequences of mutating two conserved beta-bridge forming residues in the translocation cycle of a neuronal glutamate transporter.” eng. In: *J Biol Chem* 281.38 (Sept. 2006), pp. 27905–27915.

- [48] H.J.C. Berendsen, D. van der Spoel, and R. van Drunen. “GROMACS: A message-passing parallel molecular dynamics implementation”. In: *Computer Physics Communications* 91.1-3 (Sept. 1995), pp. 43–56.
- [49] Mark James Abraham et al. “GROMACS: High performance molecular simulations through multi-level parallelism from laptops to supercomputers”. In: *SoftwareX* 1-2 (Sept. 2015), pp. 19–25.
- [50] Kresten Lindorff-Larsen et al. “Improved side-chain torsion potentials for the Amber ff99SB protein force field.” eng. In: *Proteins* 78.8 (June 2010), pp. 1950–1958.
- [51] In Suk Joung and Thomas E Cheatham 3rd. “Determination of alkali and halide monovalent ion parameters for use in explicitly solvated biomolecular simulations.” eng. In: *J Phys Chem B* 112.30 (July 2008), pp. 9020–9041.
- [52] H. J. C. Berendsen, J. R. Grigera, and T. P. Straatsma. “The missing term in effective pair potentials”. In: *The Journal of Physical Chemistry* 91.24 (Nov. 1987), pp. 6269–6271.
- [53] Kyle A Beauchamp et al. “Are Protein Force Fields Getting Better? A Systematic Benchmark on 524 Diverse NMR Measurements.” In: *Journal of chemical theory and computation* 8 (4 2012), pp. 1409–1414.
- [54] András Fiser and Andrej Šali. “Modeller: Generation and Refinement of Homology-Based Protein Structure Models”. In: *Macromolecular Crystallography, Part D* (2003), pp. 461–491.
- [55] O. Berger, O. Edholm, and F. Jähnig. “Molecular dynamics simulations of a fluid bilayer of dipalmitoylphosphatidylcholine at full hydration, constant pressure, and constant temperature”. In: *Biophysical Journal* 72.5 (May 1997), pp. 2002–2013.
- [56] Maarten G. Wolf et al. “g_membed: Efficient insertion of a membrane protein into an equilibrated lipid bilayer with minimal perturbation”. In: *Journal of Computational Chemistry* 31.11 (Mar. 2010), pp. 2169–2174.
- [57] H. J. C. Berendsen et al. “Molecular dynamics with coupling to an external bath”. In: *The Journal of Chemical Physics* 81.8 (1984), p. 3684.

- [58] M. Parrinello. “Polymorphic transitions in single crystals: A new molecular dynamics method”. In: *Journal of Applied Physics* 52.12 (1981), p. 7182.
- [59] Giovanni Bussi, Davide Donadio, and Michele Parrinello. “Canonical sampling through velocity rescaling”. In: *The Journal of Chemical Physics* 126.1 (2007), p. 014101.
- [60] Shuichi Miyamoto and Peter A. Kollman. “Settle: An analytical version of the SHAKE and RATTLE algorithm for rigid water models”. In: *Journal of Computational Chemistry* 13.8 (Oct. 1992), pp. 952–962.
- [61] Berk Hess. “P-LINCS: A Parallel Linear Constraint Solver for Molecular Simulation”. In: *Journal of Chemical Theory and Computation* 4.1 (Jan. 2008), pp. 116–122.
- [62] Sebastian Stolzenberg, George Khelashvili, and Harel Weinstein. “Structural intermediates in a model of the substrate translocation path of the bacterial glutamate transporter homologue Glt_{Ph}.” In: *The Journal of Physical Chemistry. B* 116 (18 2012), pp. 5372–5383.
- [63] Ulrich Essmann et al. “A smooth particle mesh Ewald method”. In: *The Journal of Chemical Physics* 103.19 (Nov. 1995), pp. 8577–8593.
- [64] K. Anton Feenstra, Berk Hess, and Herman J. C. Berendsen. “Improving efficiency of large time-scale molecular dynamics simulations of hydrogen-rich systems”. In: *Journal of Computational Chemistry* 20.8 (June 1999), pp. 786–798.
- [65] Dorian Krause and Philipp Thörnig. “JURECA: General-purpose supercomputer at Jülich Supercomputing Centre”. In: *Journal of large-scale research facilities JLSRF* 2 (Mar. 2016).
- [66] G.M. Torrie and J.P. Valleau. “Nonphysical sampling distributions in Monte Carlo free-energy estimation: Umbrella sampling”. In: *Journal of Computational Physics* 23.2 (Feb. 1977), pp. 187–199.
- [67] Shankar Kumar et al. “THE weighted histogram analysis method for free-energy calculations on biomolecules. I. The method”. In: *Journal of Computational Chemistry* 13.8 (Oct. 1992), pp. 1011–1021.

- [68] Jochen S. Hub, Bert L. de Groot, and David van der Spoel. “g_wham—A Free Weighted Histogram Analysis Implementation Including Robust Error and Autocorrelation Estimates”. In: *Journal of Chemical Theory and Computation* 6.12 (Dec. 2010), pp. 3713–3720.
- [69] James C. Gumbart, Benoît Roux, and Christophe Chipot. “Standard Binding Free Energies from Computer Simulations: What Is the Best Strategy?” In: *Journal of Chemical Theory and Computation* 9.1 (Jan. 2013), pp. 794–802.
- [70] Jochen S. Hub et al. “Quantifying Artifacts in Ewald Simulations of Inhomogeneous Systems with a Net Charge”. In: *Journal of Chemical Theory and Computation* 10.1 (Jan. 2014), pp. 381–390.
- [71] Vytautas Gapsys et al. “pmx: Automated protein structure and topology generation for alchemical perturbations.” eng. In: *J Comput Chem* 36.5 (Feb. 2015), pp. 348–354.
- [72] Maik Goette and Helmut Grubmüller. “Accuracy and convergence of free energy differences calculated from nonequilibrium switching processes.” eng. In: *J Comput Chem* 30.3 (Feb. 2009), pp. 447–456.
- [73] Gavin E. Crooks. “Nonequilibrium Measurements of Free Energy Differences for Microscopically Reversible Markovian Systems”. In: *Journal of Statistical Physics* 90.5/6 (1998), pp. 1481–1487.
- [74] Jan-Philipp Machtens et al. “Gating Charge Calculations by Computational Electrophysiology simulations”. In: *Biophysical Journal* (in press).
- [75] Carsten Kutzner et al. “Insights into the function of ion channels by computational electrophysiology simulations.” In: *Biochimica et Biophysica Acta* 1858 (7 Pt B 2016), pp. 1741–1752.
- [76] Robert E. Kingston, Claudia A. Chen, and Hiroto Okayama. “Calcium Phosphate Transfection”. In: *Current Protocols in Cell Biology* (Aug. 2003).
- [77] Peter Jonas. “Fast Application of Agonists to Isolated Membrane Patches”. In: *Single-Channel Recording* (1995), pp. 231–243.
- [78] Moran Jerabek-Willemsen et al. “MicroScale Thermophoresis: Interaction analysis and beyond”. In: *Journal of Molecular Structure* 1077 (Dec. 2014), pp. 101–113.

- [79] B. Efron. “Bootstrap Methods: Another Look at the Jackknife”. In: *The Annals of Statistics* 7.1 (Jan. 1979), pp. 1–26.
- [80] H.H. Ku. “Notes on the use of propagation of error formulas”. In: *Journal of Research of the National Bureau of Standards, Section C: Engineering and Instrumentation* 70C.4 (Oct. 1966), p. 263.
- [81] Schrödinger, LLC. “The PyMOL Molecular Graphics System, Version 1.8”. Nov. 2015.
- [82] Sonja Jensen et al. “Crystal structure of a substrate-free aspartate transporter.” eng. In: *Nat Struct Mol Biol* 20.10 (Oct. 2013), pp. 1224–1226.
- [83] Germano Heinzemann and Serdar Kuyucak. “Molecular dynamics simulations of the mammalian glutamate transporter EAAT3.” eng. In: *PLoS One* 9.3 (2014), e92089.
- [84] David C. Holley and Michael P. Kavanaugh. “Interactions of alkali cations with glutamate transporters.” eng. In: *Philos Trans R Soc Lond B Biol Sci* 364.1514 (Jan. 2009), pp. 155–161.
- [85] Zhijian Huang and Emad Tajkhorshid. “Dynamics of the Extracellular Gate and Ion-Substrate Coupling in the Glutamate Transporter”. In: *Biophysical Journal* 95.5 (Sept. 2008), pp. 2292–2300.
- [86] D. Ewers et al. “Induced fit substrate binding to an archeal glutamate transporter homologue”. In: *Proceedings of the National Academy of Sciences* 110.30 (July 2013), pp. 12486–12491.
- [87] Inga Hänelt et al. “Low Affinity and Slow Na⁺ Binding Precedes High Affinity Aspartate Binding in the Secondary-active Transporter Glt_{Ph}.” eng. In: *J Biol Chem* 290.26 (June 2015), pp. 15962–15972.
- [88] Nicolas Reyes, SeCheol Oh, and Olga Boudker. “Binding thermodynamics of a glutamate transporter homolog”. In: *Nature Structural & Molecular Biology* 20.5 (Apr. 2013), pp. 634–640.
- [89] Jacques I. Wadiche and Michael P. Kavanaugh. “Macroscopic and Microscopic Properties of a Cloned Glutamate Transporter/Chloride Channel”. In: *Journal of Neuroscience* 18.19 (1998), pp. 7650–7661.

- [90] Keiko Shimamoto et al. “dl-threo- β -Benzyloxyaspartate, A Potent Blocker of Excitatory Amino Acid Transporters”. In: *Molecular Pharmacology* 53.2 (1998), pp. 195–201.
- [91] Christof Grewer et al. “Charge compensation mechanism of a Na⁺-coupled, secondary active glutamate transporter.” eng. In: *J Biol Chem* 287.32 (Aug. 2012), pp. 26921–26931.
- [92] Ameer N Thompson et al. “Mechanism of potassium-channel selectivity revealed by Na⁺ and Li⁺ binding sites within the KcsA pore”. In: *Nature Structural & Molecular Biology* 16.12 (Nov. 2009), pp. 1317–1324.
- [93] C. Grewer. “Is the Glutamate Residue Glu-373 the Proton Acceptor of the Excitatory Amino Acid Carrier 1?” In: *Journal of Biological Chemistry* 278.4 (Nov. 2002), pp. 2585–2592.
- [94] Germano Heinzelmann and Serdar Kuyucak. “Molecular dynamics simulations elucidate the mechanism of proton transport in the glutamate transporter EAAT3.” eng. In: *Biophys J* 106.12 (June 2014), pp. 2675–2683.
- [95] Nurunisa Akyuz et al. “Transport domain unlocking sets the uptake rate of an aspartate transporter.” eng. In: *Nature* 518.7537 (Feb. 2015), pp. 68–73.
- [96] Ariane Leinenweber et al. “Regulation of glial glutamate transporters by C-terminal domains.” eng. In: *J Biol Chem* 286.3 (Jan. 2011), pp. 1927–1937.
- [97] B. Billups, D. Rossi, and D. Attwell. “Anion conductance behavior of the glutamate uptake carrier in salamander retinal glial cells.” eng. In: *J Neurosci* 16.21 (Nov. 1996), pp. 6722–6731.
- [98] Y. Zhou et al. “EAAT2 (GLT-1; slc1a2) Glutamate Transporters Reconstituted in Liposomes Argues against Heteroexchange Being Substantially Faster than Net Uptake”. In: *Journal of Neuroscience* 34.40 (Oct. 2014), pp. 13472–13485.

- [99] Dwight E. Bergles, Anastassios V. Tzingounis, and Craig E. Jahr. “Comparison of coupled and uncoupled currents during glutamate uptake by GLT-1 transporters.” eng. In: *J Neurosci* 22.23 (Dec. 2002), pp. 10153–10162.
- [100] Inga Hänelt et al. “Conformational heterogeneity of the aspartate transporter Glt_{PH}.” eng. In: *Nat Struct Mol Biol* 20.2 (Feb. 2013), pp. 210–214.
- [101] Noa Rosental et al. “A conserved aspartate residue located at the extracellular end of the binding pocket controls cation interactions in brain glutamate transporters.” eng. In: *J Biol Chem* 286.48 (Dec. 2011), pp. 41381–41390.
- [102] Christoph Fahlke, Daniel Kortzak, and Jan-Philipp Machtens. “Molecular physiology of EAAT anion channels”. In: *Pflügers Archiv - European Journal of Physiology* 468.3 (Dec. 2015), pp. 491–502.
- [103] Rose Tanui et al. “Electrogenic Steps Associated with Substrate Binding to the Neuronal Glutamate Transporter EAAC1”. In: *J. Biol. Chem.* 291.22 (Apr. 2016), pp. 11852–11864.

9. Publications

During my PhD project I contributed to the following peer-reviewed publications:

- Jan-Philipp Machtens, Daniel Kortzak, Christine Lansche, Ariane Leinenweber, Petra Kilian, Birgit Begemann, Ulrich Zachariae, David Ewers, Bert L. de Groot, Rodolfo Briones, and Christoph Fahlke. “Mechanisms of anion conduction by coupled glutamate transporters.” In: *Cell* 160.3 (Jan. 2015), pp. 542–553.

Author’s contribution statement: I performed and analyzed patch-clamp recordings to investigate cation/anion selectivity and applied advanced noise analysis techniques to quantify single-channel conductances of EAAT anion channels. I contributed to writing the manuscript.

- Christoph Fahlke, Daniel Kortzak, and Jan-Philipp Machtens. “Molecular physiology of EAAT anion channels”. In: *Pflügers Archiv - European Journal of Physiology* 468.3 (Dec. 2015), pp. 491–502.

Author’s contribution statement: I contributed the patch-clamp recordings and the analysis for estimation of the absolute open probability of EAAT anion channels. I contributed to writing the manuscript.

10. Abbreviations

Arg	R	Arginine
His	H	Histidine
Lys	K	Lysine
Asp	D	Aspartic acid
Glu	E	Glutamic acid
Asn	N	Asparagine
Cys	C	Cysteine
Gln	Q	Glutamine
Gly	G	Glycine
Ser	S	Serine
Thr	T	Threonine
Tyr	Y	Tyrosine
Ala	A	Alanine
Ile	I	Isoleucine
Leu	L	Leucine
Met	M	Methionine
Phe	F	Phenylalanine
Pro	P	Proline
Trp	W	Tryptophan
Val	V	Valine

EAAT	excitatory amino acid transporter
EGTA	(ethylene glycol-bis(β -aminoethyl ether)-N,N,N',N'-tetraacetic acid
Glt _{Ph}	aspartate transporter from <i>Pyrococcus horikoshii</i>
HEK	human embryonic kidney cell
HEPES	(4-(2-hydroxyethyl)-1-piperazineethanesulfonic acid)
HP	hairpin
NMDG	N-Methyl-D-glucamine
MD	molecular dynamics
MST	microscale thermophoresis
PME	particle mesh Ewald
PMF	potential of mean force
SD	standard deviation
TBOA	dl-threo- β -benzyloxyaspartate
TEA	tetraethylammonium
TM	transmembrane helix

11. Eidesstattliche Versicherung

Ich versichere an Eides Statt, dass die Dissertation von mir selbstständig und ohne unzulässige fremde Hilfe unter Beachtung der “Grundsätze zur Sicherung guter wissenschaftlicher Praxis an der Heinrich-Heine-Universität Düsseldorf” erstellt worden ist. Jülich, 2017

Ort,Datum

Daniel Kortzak

12. Danksagung

An erster Stelle möchte ich meinem Doktorvater Herrn Prof. Christoph Fahlke für die großzügige Überlassung des Themas, die intensive Betreuung, viel Verständnis und die Kühnheit, einen Mathematiker in sein Labor aufzunehmen, danken. Herrn Prof. Holger Gohlke danke ich dafür, dass er das Zweitgutachten dieser Arbeit übernommen hat.

Bei Jan-Philipp Machtens bedanke ich mich dafür, dass er mir als mein Betreuer jederzeit mit Rat und Tat zur Seite stand.

Des Weiteren möchte ich mich bei Ingo Weyand und Meike Zimmermann für die MST Experimente bedanken, bei Gabriel Stölting und Peter Kovermann für viel Geduld beim Lehren des Patchen, ebenso bei Prof. Arnd Baumann und Joachim Schmitz für ähnlich viel Geduld in der Zellkultur. Petra Thelen und Arne Franzen danke ich für die Übernahme der Molekularbiologie.

Zu guter letzt danke ich allen anderen Mitarbeitern des ICS-4 für die kollegiale Zusammenarbeit in den letzten Jahren.